WDR90 is a centriolar microtubule wall protein important for centriole architecture integrity.

Emmanuelle Steib[1], Davide Gambarotto[1†], Marine Laporte[1†], Natacha Olieric[2], Céline Zheng[2*], Susanne Borgers[1], Vincent Olieric[3], Maeva Le Guennec[1], France Koll[4], Anne-Marie Tassin[4], Michel O. Steinmetz[2,5], Paul Guichard[1§] and Virginie Hamel[1§]

[1] University of Geneva, Department of Cell Biology, Sciences III, Geneva, Switzerland

[2] Laboratory of Biomolecular Research, Division of Biology and Chemistry, Paul Scherrer Institut, Villigen, Switzerland

[3] Swiss Light Source, Paul Scherrer Institut, 5232 Villigen, Switzerland

[4] Institute for Integrative Biology of the Cell (I2BC), CEA, CNRS, Univ. Paris Sud, Université Paris-Saclay, 1 Avenue de la Terrasse, 91198 Gif sur Yvette, France.

[5] Biozentrum, University of Basel, 4056 Basel, Switzerland

* Present address: Department of Biochemistry, University of Oxford, South Parks Road, Oxford, OX1 3QU, UK

[†] These authors contributed equally to this work.

§ Correspondence to: virginie.hamel@unige.ch and paul.guichard@unige.ch

Summary

Centrioles are characterized by a nine-fold arrangement of long-lived microtubule triplets that are held together by an inner protein scaffold. These structurally robust organelles experience strenuous cellular processes such as cell division or ciliary beating while performing their function. However, the molecular mechanisms underlying the stability of microtubule triplets, as well as centriole architectural integrity remain poorly understood. Here, using ultrastructure expansion microscopy (U-ExM) for nanoscale protein mapping, we reveal that POC16 and its human homolog WDR90 are components of the centriolar microtubule wall along the central core region of the centriole. We further found that WDR90 is an evolutionary microtubule associated protein with a predicted structurally homology with the ciliary inner junction protein FAP20. Finally, we demonstrate that WDR90 depletion impairs the localization of inner scaffold components, leading to centriole structural abnormalities in both human and *Chlamydomonas* cells. Altogether, this work highlights that POC16/WDR90 is a crucial evolutionary conserved molecular player participating in centriole architecture integrity.

Keywords: centriole, inner scaffold, *Chlamydomonas*, human cells, Ultrastructure Expansion Microscopy, microtubules.

Introduction

Centrioles and basal bodies (referred to as centrioles from here onwards for simplicity) are conserved organelles important for the formation of the centrosome as well as for templating cilia and flagella assembly (Bornens, 2012; Breslow and Holland, 2019; Conduit et al., 2015; Ishikawa and Marshall, 2011). Consequently, defects in centriole assembly, size, structure and number lead to abnormal mitosis or defective ciliogenesis and have been associated with several human pathologies such as ciliopathies and cancer (Gönczy, 2015; Nigg and Holland, 2018; Nigg and Raff, 2009). For instance, centriole amplification, a hallmark of cancer cells, can result from centriole fragmentation in defective, over-elongated centrioles (Marteil et al., 2018).

Centrioles are characterized by a nine-fold radial arrangement of microtubule triplets, are polarized along their long axis, and can be divided in three distinct regions termed proximal end, central core and distal tip (Hamel et al., 2017). Each region displays specific structural features such as the cartwheel on the proximal end, which is crucial for centriole assembly (Nakazawa et al., 2007; Strnad et al., 2007) or the distal appendages at the very distal region, essential for membrane docking during ciliogenesis (Tanos et al., 2013). The central core region of the centriole is defined by the presence of a circular inner scaffold thought to maintain the integrity of microtubule triplets under compressive forces (Le Guennec et al., 2020). Using cryo-tomography, we recently showed that the inner centriole scaffold forms an extended helix covering ~70% of the centriole length and that is rooted at the inner junction between the A and B microtubules (Figure 1A, B). This connection consists of a stem attaching the neighboring A and B microtubules and three arms extending from the same stem toward the centriolar lumen (Le Guennec et al., 2020) (Figure 1A, B). The stem of the inner scaffold has been detected in *Paramecium tetraurelia*, *Chlamydomonas reinhardtii* and

human centrioles, suggesting that it represents an evolutionary conserved structural feature.

The molecular identity of some components of the inner scaffold has been uncovered using Ultrastructure Expansion Microscopy (U-ExM), which allows nanoscale localization of proteins within structural elements (Gambarotto et al., 2019). Notably, the centriolar proteins POC1B, FAM161A, POC5 and Centrin-2 have been shown to localize to the inner scaffold along the microtubule blades in human cells (Le Guennec et al., 2020). Moreover, these proteins form a complex that can bind to microtubules through the microtubule-binding protein FAM161A (Le Guennec et al., 2020; Zach et al., 2012). Importantly, a subset of these proteins has been shown to be important, such as POC5 for centriole elongation (Azimzadeh et al., 2009) as well as POC1B for centriole and basal body integrity (Pearson et al., 2009; Venoux et al., 2013). This observation highlights the role of the inner scaffold structure in providing stability to the entire centriolar microtubule wall organization. However, the exact contribution of the inner scaffold to microtubule triplets stability and how the inner scaffold is connected to the microtubule blade is unknown.

We recently identified the conserved proteins POC16/WDR90 as proteins localizing to the central core region in both *Chlamydomonas reinhardtii* and human centrioles (Hamel et al., 2017). Impairing POC16 or WDR90 functions has been found to affect ciliogenesis, suggesting that POC16/WDR90 may stabilize the microtubule wall, thereby ensuring proper flagellum or cilium assembly (Hamel et al, 2017). Interestingly, POC16 has been proposed to be at the inner junction between the A and B microtubules (H. Yanagisawa et al., 2014) through its sequence homology with FAP20, an axonemal microtubule doublet inner junction protein of *Chlamydomonas reinhardtii* flagella (Dymek et al., 2019; Ma et al., 2019; Owa et al., 2019; H. A.

Yanagisawa et al., 2014). As the stem connects the A- and B-microtubules interface, these observations suggest that POC16/WDR90 may connect the inner scaffold to the microtubule triplet through this stem structure (Figure 1C), thus ensuring integrity of the centriole architecture.

In this study, using a combination of cell biology, biochemistry and Ultrastructure Expansion Microscopy (U-ExM) approaches, we establish that the conserved POC16/WDR90 proteins localize on the centriolar microtubule wall in the central core region of both *Chlamydomonas* and human cells. We further demonstrate that WDR90 is a microtubule-binding protein and that loss of this protein impairs the localization of inner scaffold components and leads to slight centriole elongation, impairment of the canonical circular shape of centrioles as well as defects in centriolar architecture integrity.

Results

POC16/WDR90 is a conserved microtubule wall component of the central core region

To test the hypothesis that POC16/WDR90 is a microtubule triplet component, we analyzed its distribution using U-ExM that allows nanoscale mapping of proteins inside the centriole (Gambarotto et al., 2019; Le Guennec et al., 2020). We observed first in *Chlamydomonas reinhardtii* isolated centrioles that the endogenous POC16 longitudinal fluorescence signal is restricted to the central core region as compared to the tubulin signal, which depicts total centriolar length (Figure 1D-F). From top viewed centrioles, we measured both POC16 and tubulin maximal intensity signal from the exterior to the interior of the centriole and quantified the distance between x-values

125 (Figure 1M, N, average distance between POC16 and tubulin Δ = 0 nm +/- 8). We
126 concluded that POC16 localizes precisely on the microtubule wall in the central core
127 region of *Chlamydomonas* centrioles. As a control, we could recapitulate the internal
128 localization along the microtubule wall of POB15, another central core protein (Figure
129 1G-I and Figure 1M, N, average distance between POB15 and tubulin Δ = 12 nm +/-
130 7) as previously reported using immunogold-labeling (Hamel et al., 2017). In human
131 centrioles, the POC16 human homolog WDR90 localizes similarly to POC16 on the
132 centriolar microtubule wall, demonstrating the evolutionary conserved restricted
133 localization of POC16/WDR90 on microtubule triplets in the central core region of
134 centrioles (Figure 1J-L). Of note, POC16 and WDR90 display a punctate distribution
135 that we hypothesize to be due to the poor quality of the antibody.

136 Next, we compared the relative position of WDR90 to previously described
137 inner scaffold components (Figure 1O-Q). We found that while WDR90 precisely
138 localizes to the centriolar microtubule wall (Figure 1P, average distance between
139 WDR90 and tubulin: Δ= 2nm +/ 12), POC1B, FAM161A, POC5 and Centrin-2 signals
140 were shifted towards the centriole lumen in comparison to the tubulin signal, as
141 previously reported (Figure 1P, Δ= 15nm +/- 8; 22nm +/- 5; 27nm +/- 6 and 28nm +/-
142 9, respectively) (Le Guennec et al., 2020). These results demonstrate that WDR90
143 longitudinal localization is similar to the inner scaffold components but that WDR90
144 localizes on the microtubule triplet. This result suggests that WDR90 is a component
145 of the centriolar microtubule triplet of the central core region.

146

147 **POC16/WDR90 is an evolutionary conserved microtubule associated protein**

148 Proteins of the POC16/WDR90 family consist of an N-terminal DUF667-
149 containing domain (domain of unknown function), homologous to the ciliary inner

junction protein FAP20 (Figure S1A) (Yanagisawa et al., 2014), which is followed by multiple WD40 repeats that form β-propeller structures (Figure 2A and Figure S1B) (Xu and Min, 2011).

First, we wanted to probe the evolutionary conservation of POC16/WDR90 family members as centriolar proteins. To this end, we raised an antibody against *Paramecium tetraurelia* POC16 and confirmed its localization at centrioles similarly to what we found in *Chlamydomonas reinhardtii* and human cells (Figure S1C) (Hamel et al., 2017).

Further driven by its predicted homology to the microtubule associated protein FAP20 (Khalifa et al., 2019) and the underlying hypothesis that POC16/WDR90 proteins might be joining A and B microtubules as well as by their precise localization on the microtubule wall (Figure 1), we first set out to understand the structural homology between the predicted structures of POC16-DUF667 domain to the recently published near atomic structure of FAP20 from flagella microtubule doublets (Khalifa et al., 2020; Ma et al., 2019) (Figure S2A-C). Strikingly, we observed high similarities between the two structures, suggesting similar biological functions at the inner junction. Moreover, we fitted POC16 model prediction into FAP20 cryo-EM density map and found a good concordance, further hinting for a conserved localization at the level of the microtubule triplet (Figure S2D).

Prompted by this result, we then tested whether POC16/WDR90 proteins, similar to FAP20, can bind microtubules both in human cells as well as *in vitro*. To do so, we overexpressed the N-terminal part of WDR90 and crPOC16 comprising the DUF667 domain (WDR90-N(1-225) and CrPOC16(1-295), respectively) fused to GFP in U2OS cells and found that this region is sufficient to decorate cytoplasmic microtubules (Figures 2B and S3A). We next tested whether overexpressing such a

175 WDR90-N-terminal fragment could stabilize microtubules. To this end, we analyzed
176 the microtubule network in cells overexpressing mCherry-WDR90-N after
177 depolymerizing microtubules through a cold shock treatment (Figure S3B-D). We
178 found that while low expressing cells did not maintain a microtubule network, high
179 expressing cells did. This suggests that WDR90-N can stabilize microtubules. In
180 contrast, we observed that full-length WDR90 fused to GFP only anecdotally binds
181 microtubules. This observation suggests a possible autoinhibition conformation of the
182 full-length protein and/or to interacting partners preventing microtubule binding in the
183 cytoplasm (Figure S3E).

184 Next, we determined whether different POC16/WDR90 N-terminal domains
185 directly bind to microtubules *in vitro* and whether this function has been conserved in
186 evolution. Bacterially expressed, recombinant POC16/WDR90 DUF667 domains from
187 seven different species were purified and their microtubule interaction ability was
188 assessed using a standard microtubule-pelleting assay (Figure S1A and Figure 2C). We
189 found that every POC16/WDR90 DUF667 domain directly binds to microtubules *in*
190 *vitro*. This interaction was further confirmed using negative staining electron
191 microscopy, where we could observe recombinant WDR90-N localizing on *in vitro*
192 polymerized microtubules (Figure 2E).

193 We next investigated whether POC16/WDR90 DUF667 domain could also
194 interact with free tubulin dimers, considering that closure of the inner junction between
195 the A and B microtubules necessitates two microtubule/tubulin-binding sites as recently
196 reported for FAP20 (Ma et al., 2019). We observed that all POC16/WDR90 DUF667
197 orthologs directly interact with tubulin dimers, generating oligomers that pellet under
198 centrifugation (Figure 2D). We then tested whether the DUF667 domain could still
199 interact with tubulin once bound to microtubules. We subsequently incubated either

200 WDR90-N or crPOC16(1-295) pre-complexed with microtubules with an excess of free
201 tubulin and analyzed their structural organization by electron microscopy (Figure 2E,
202 F and Figure S3F, G). We observed an additional level of decoration due to the
203 simultaneous binding of the DUF667 domains with tubulin and microtubules (Figure
204 2E, F and Figure S3F, G). Furthermore, we revealed a 8.5 nm periodical organization
205 of tubulin-WDR90-N oligomers on microtubules (Figure 2G), similar to the recent
206 high-resolution structure of the ciliary microtubule doublet showing that monomeric
207 FAP20 interacts with both A- and B-microtubules every 8nm at the inner junction
208 (Khalifa et al., 2020; Ma et al., 2019). In this context, it is tempting to speculate that
209 the DUF667 domain of POC16/WDR90 is also monomeric, however it is also possible
210 that WDR90 forms a homodimer capable of interacting with the microtubules and
211 tubulin.

212 Based on these results, we concluded that POC16/WDR90 is an evolutionary
213 conserved microtubule/tubulin-interacting protein with the capacity to connect
214 microtubules, a functional prerequisite for an inner junction protein that simultaneously
215 interacts with the A and B microtubules.

216

217 **WDR90 is recruited in G2 during centriole core elongation**

218 We next assessed whether WDR90 recruitment at centrioles is correlated with
219 the appearance of inner scaffold proteins during centriole biogenesis. Centrioles
220 duplicate only once per cell cycle during S phase, with the appearance of one
221 procentriole orthogonally to each of the two mother centrioles. Procentrioles then
222 elongate during the following G2 phase of the cell cycle, acquiring the inner scaffold
223 protein POC5 that is critical for the formation of the central and distal parts of the
224 nascent procentriole (Azimzadeh et al., 2009). We followed endogenous WDR90

225 localization across the cell cycle by analyzing synchronized human RPE1 cells fixed at
226 given time points and stained for either Centrin-2 or HsSAS-6, both early protein
227 marker of duplicating centrioles (Azimzadeh et al., 2009; Strnad et al., 2007) (Figure
228 3A-F and Figure S4A, B). We found that while Centrin-2 and HsSAS-6 are recruited
229 as expected early on during procentriole formation in S phase, WDR90 starts appearing
230 only in early G2 when procentriole elongation starts (Figure 3A-F). Signal intensity
231 analysis over the cell cycle further demonstrates that WDR90 appears on procentrioles
232 in early G2 and reaches full incorporation by the end of G2 (Figure 3G, H), similarly
233 to the reported incorporation of the inner scaffold protein POC5 (Azimzadeh et al.,
234 2009).

235 Moreover, we noticed that besides its centriolar distribution, WDR90 localizes
236 also to centriolar satellites, which are macromolecular assemblies of centrosomal
237 proteins scaffolded by the protein PCM1 and involved in centrosomal homeostasis
238 (Drew et al., 2017) (Figure S4C-H). Thus, we tested whether WDR90 satellite
239 localization depends on the satellite protein PCM1 by depleting PCM1 using siRNA
240 and assessing WDR90 distribution. We found that in absence of PCM1, WDR90 is
241 solely found at centrioles (Figure S4E-H), demonstrating that WDR90 satellite
242 localization is PCM1-dependent.

243 Altogether, these data establish that WDR90 is a centriolar and satellite protein
244 that is recruited to centrioles in the G2-phase of the cell cycle, during procentriole
245 elongation and central core/distal formation, similarly to the recruitment of the inner
246 scaffold protein POC5.

247

248 **WDR90 is important to recruit Centrin-2 and POC5**

249 To better understand the function of WDR90, we analyzed cycling human cells
250 depleted for WDR90 using siRNA and co-labeled WDR90 with either the early
251 centriolar marker Centrin-2 or the G2-marker POC5. As previously shown (Hamel et
252 al., 2017), WDR90 siRNA-treated cells showed significantly reduced WDR90 levels at
253 centrosomes in comparison to control cells (Figure S5A, C). Moreover, we observed
254 an asymmetry in signal reduction at centrioles in WDR90-depleted cells, with only one
255 of two Centrin-2 positive centrioles still associated with WDR90 in G1 and early S-
256 phase (69% compared to 10% in controls) and one of four Centrin-2 positive centrioles
257 in S/G2/M cells (77% compared to 0% in controls, Figure S5B). As the four Centrin-2
258 positive dots indicate duplicated centrioles, this result suggests that the loss of WDR90
259 does not result from a duplication failure (Figure S5B). We postulate that the remaining
260 WDR90 signal possibly corresponds to the mother centriole and that the daughter has
261 been depleted from WDR90 (Figure S5E), similarly to what has been observed for the
262 protein POC5 (Azimzadeh et al., 2009). We further conclude that WDR90 is stably
263 incorporated into centrioles, in agreement with its possible structural role.
264 We also noted that the intensity of the Centrin-2 and POC5 signals were
265 markedly reduced upon WDR90 siRNA treatment (Figure S5D-K). Indeed, we found
266 that only 39% of WDR90-depleted cells displayed 2 POC5 dots in G1 (negative for
267 HsSAS-6 signal) in contrast to the 86% of control cells with 2 POC5 dots (Figure S5H).
268 Moreover, 68% of control cells had 2 to 4 POC5 dots in S/G2/M (associated with 2
269 HsSAS-6 dots) in contrast to 29% in WDR90-depleted condition (Figure S5H). The
270 HsSAS-6 signal was not affected in WDR90-depleted cells, confirming that initiation
271 of the centriole duplication process is not impaired under this condition (Figure S5G, J,
272 L). Similarly, the fluorescence intensity of the distal centriole cap protein CP110 was
273 not changed under WDR90-depletion in contrast to the Centrin-2 signal reduction (Fig

274 S5M-O). These results establish that the localization of Centrin-2 and POC5, two
275 components of the inner scaffold, are affected upon WDR90 depletion in contrast to the
276 proximal protein HsSAS-6 and distal cap protein CP110.

277 To ascertain this phenotype, we generated a stable cell line expressing a siRNA-
278 resistant version of WDR90 fused to GFP in its N-terminus (GFP-WDR90RR) upon
279 doxycycline induction. We found that expression of GFP-WDR90RR restores partially
280 the Centrin-2 and POC5 signals at centrioles (Figure 3I- L).

281 Taken together, these results indicate that the depletion of WDR90 leads to a
282 decrease in Centrin-2 and POC5 localization at centrioles but does not affect the
283 initiation of centriole duplication nor the recruitment of the distal cap protein CP110.

284

285 ***Chlamydomonas* POC16 is crucial to maintain centriole core integrity**

286 To investigate the structural role of POC16/WDR90 proteins on centrioles, we
287 initially turned to the *Chlamydomonas reinhardtii poc16m504* mutant generated by the
288 Chlamy Library project (Li et al., 2016), which contains an insertion of a CIB1 cassette
289 in the *poc16* genomic sequence (Hamel et al., 2017). We demonstrated previously that
290 this mutant is not a null, but has reduced amount of POC16 proteins detected at
291 centrioles and displays flagella defects with 80% of mutant cells bearing 0, 1 or
292 impaired flagella (Figure S6A-C) (Hamel et al., 2017). We hypothesized from these
293 results that a POC16 truncated protein is made, although this could not be confirmed,
294 as POC16 antibodies do not detect the 230kDa endogenous protein in centriolar extracts
295 by Western Blot (Hamel et al., 2017). Here, we confirmed, by performing
296 immunofluorescence analysis of wild-type and *poc16m504 Chlamydomonas* cells co-
297 stained for POC16 and tubulin, that the overall POC16 levels at centrioles were reduced
298 (Figure 4A, B). Moreover, we noticed that 52% of *poc16m504* centriole pairs had only

299 one detectable POC16 dot and 25% had none as compared to the 2 POC16 dots in the
300 wild-type (Figure 4C). In contrast, by staining for the cartwheel component Bld12
301 (Nakazawa et al., 2007), we found that the fluorescent signal was similar to wild-type
302 in this background, suggesting that the proximal region of the centriole is not affected
303 (Figure S6D-F), similarly to human cells.

304 To assess whether the ultrastructure and in particular the central core region of
305 centrioles in *poc16m504* cells was defective, we analyzed this mutant using electron
306 microscopy of resin-embedded specimens (Figure 4D-H). We first noticed that the
307 *poc16m504* mutant displayed shorter centrioles with an average length of 370 nm (+/-
308 7 nm) compared to 460 nm (+/- 9 nm) in the wild type (Figure 4D, E). Moreover, we
309 found that the stellate fibers present in the transition zone of wild-type centrioles
310 (Figure 4D, white star) (Geimer and Melkonian, 2004), are ectopically localized to the
311 central core region of *poc16m504* mutants in 46% of the cases (Figure 4D, F-H, red
312 star). This additional localization of stellate fibers has previously been described for the
313 δ-tubulin mutant *uni*-3, which also displays defective microtubule triplets (O'Toole et
314 al., 2003). However, in contrast to *uni-3*, we noted that microtubule triplets were
315 apparently not affected in the *poc16m504* mutant (Figure 4G). However, even if
316 extremely rare owing to the difficulty to obtain a perfect longitudinal view of the
317 centriole in the resin-embedded sections, we observed a centriole with a broken
318 microtubule wall at the level of the central core region, suggestive of centriole fracture
319 (Figure 4H, arrow).

320 To better characterize this phenotype, we turned to U-ExM that allows
321 visualization of centrioles ultrastructure in a more quantitative manner and in the
322 context of the whole organism (Gambarotto et al., 2019). While the procentrioles
323 looked intact, confirming that proximal assembly initiation is not affected in this mutant,

324 55% of the *poc16m504* mutants displayed defective mature centrioles compared to wild
325 type (Figure 4I-K and Figure S6G, H). We notably observed incomplete mature
326 centrioles lacking the entire central and distal parts, suggesting either a defect in
327 centriole assembly and elongation or an impairment of centriole stability (Figure 4I, J
328 and Figure S6G, H). Moreover, consistent with our electron microscopy analysis,
329 quantification of mature centrioles in this mutant demonstrated that centrioles are
330 shorter (Figure 4L).
331 Altogether, these results demonstrate that the central core region of *poc16m504* mutants
332 is impaired, highlighting a potential role of POC16 in either maintaining the structural
333 integrity of the microtubule wall in this region of the centriole and/or its assembly.
334

335 **WDR90 depletion leads to a loss of inner scaffold components and to centriole**
336 **fracture**

337 Based on these findings, we wondered whether WDR90 depletion might lead to
338 a loss of inner scaffold components as well as to a centriole architecture destabilization
339 in human cells. We tested this hypothesis by analyzing centrioles from WDR90-
340 depleted U2OS cells using U-ExM (Figure 5). As expected, we observed a strong
341 reduction of WDR90 at centrioles, with a reminiscent asymmetrical signal in one of the
342 two mature centrioles (Figure 5A-C). Unexpectedly, we found that WDR90-depleted
343 centrioles exhibited a slight tubulin length increase (502 nm +/- 65 compared to 434
344 nm +/- 58 in controls), potentially indicative of a defect in centriole length regulation
345 (Figure 5D). In contrast, despite a slight decrease at the level of the central core, we did
346 not observe, in neither of the conditions, any significant difference in centriole diameter
347 at the proximal and very distal regions (Figure 5E).

348 We next analyzed whether the localization of the four described inner scaffold
349 components POC1B, FAM161A, POC5 and Centrin-2 would be affected in WDR90-
350 depleted cells. We found that the localization of these four proteins in the central core
351 region of centrioles was markedly altered in WDR90-depleted centrioles (Figure 5F,
352 G). Instead of covering ~60% of the entire centriolar lumen, we only observed a ~20%
353 remaining belt, positive for inner scaffold components at the proximal extremity of the
354 core region (Figure 5F-H and Figure S7A, B), suggesting that their initial recruitment
355 may not be entirely affected. Another possibility would be that incomplete depletion of
356 WDR90 allows for partial localization of inner scaffold components. It should also be
357 noted that Centrin-2, which displays a central core and an additional distal tip
358 decoration (Le Guennec et al., 2020), was affected specifically in its inner core
359 distribution (Figure 5F, white arrow, Figure S7A, B).

360 The discovery of the inner scaffold within the centriole led to the hypothesis
361 that this structure is important for microtubule triplet stability and thus overall centriole
362 integrity (Le Guennec et al., 2020). In line with this hypothesis, we found that upon
363 WDR90 depletion, 10% of cells had their centriolar microtubule wall broken, indicative
364 of microtubule triplets fracture and loss of centriole integrity (15 out of 150 centrioles,
365 Figure 6, Videos 1 and 2). The break occurred mainly above the remaining belt of inner
366 scaffold components (Figure 6A-D), possibly reflecting a weakened microtubule wall
367 in the central and distal region of the centriole. We also noticed that the perfect
368 cylindrical shape (defined as roundness) of the centriolar microtubule wall was affected
369 with clear ovoid-shaped or opened centrioles seen from near-perfect top view oriented
370 centrioles (Figure 6E, F and Figure S7C), illustrating that loss of WDR90 and the inner
371 scaffold leads to disturbance of the characteristic centriolar architecture.

372 Collectively, these data demonstrate that WDR90 is crucial to ensure inner core
373 protein localization within the centriole core, as well as maintaining the microtubule
374 wall integrity and the overall centriole roundness and stability (Figure 6G).
375
376
377 **Discussion**
378 What maintains centriole barrel stability and roundness is a fundamental open
379 question. Centrioles are microtubule barrel structures held together by the A-C linker
380 at their proximal region and a recently discovered inner scaffold in the central/distal
381 region (Le Guennec et al., 2020). The presence of such an extended scaffold covering
382 70% of the centriolar length has led to the hypothesis that this structure is important for
383 maintaining centriole integrity (Le Guennec et al., 2020). Our work demonstrates that
384 POC16/WDR90 family proteins, which are important for cilia and flagella formation,
385 constitute an evolutionary conserved central core microtubule triplet component that is
386 essential for maintaining the inner centriolar scaffold proteins. The depletion of
387 WDR90 leads to centriolar defects and impairment of microtubule triplets organization
388 resulting in the loss of the canonical circular shape of centrioles. We also found that
389 this overall destabilization of the centriole can lead to microtubule triplet breakage.
390 Whether this phenotype arises as a consequence of the loss of the inner scaffold or due
391 to the destabilization of the inner junction of the microtubule triplet is still an opened
392 question that should be addressed in the future.
393 We demonstrate that POC16/WDR90 is a component of the microtubule triplet
394 restricted to the central core region. In addition and based on the sequence and structural
395 similarity to the DUF667 domain of FAP20 that composes the inner junction in flagella,
396 we propose that POC16/WDR90 localizes at the inner junction of the A and B

397 microtubule of the centriolar microtubule triplet. The fact that WDR90 localization is
398 restricted to the central core region led us to hypothesize that another protein, possibly
399 FAP20 as it has been previously reported at centrioles (H. Yanagisawa et al., 2014),
400 could mediate the inner junction between A- and B-microtubule in the proximal region
401 of the centriole. Moreover, in POC16/WDR90 proteins, the DUF667 domain is
402 followed by a WD40 domain sharing a homology with the flagellar inner B-microtubule
403 protein FAP52/WDR16 (Owa et al., 2019) leading us to postulate that the WD40
404 domains of POC16/WDR90 might also be located inside the B-microtubule of the
405 triplet. However, whether this is the case remains to be addressed in future studies.
406 Our work further establishes that WDR90 is recruited to centrioles in G2 phase of the
407 cell cycle concomitant with centriole elongation and inner central core assembly. We
408 found that WDR90 depletion does not impair centriole duplication nor microtubule wall
409 assembly, as noted by the presence of the proximal marker HsSAS-6 and the distal cap
410 CP110. In stark contrast, WDR90 depletion leads to a strong reduction of inner scaffold
411 components at centrioles, as well as some centriole destabilization.
412 Although several examples of centriole integrity loss have been demonstrated in the
413 past, the molecular mechanisms of centriole disruption are not understood. For instance,
414 Delta- and Epsilon-tubulin null human mutant cells were shown to lack microtubule
415 triplets and have thus unstable centrioles that do not persist to the next cell cycle (Wang
416 et al., 2017). Remarkably, these centrioles can elongate with a proper recruitment of
417 the cartwheel component HsSAS-6 and the distal marker CP110 but fails to recruit
418 POC5, a result that is similar to our findings with WDR90 depleted cells. As Delta- and
419 Epsilon-tubulin null human mutant cells can solely assemble microtubule singlets
420 (Wang et al., 2017), we speculate that WDR90 might not be recruited in these centrioles,
421 as the A-and B-microtubule inner junction would be missing. As a consequence, the

422 inner scaffold proteins will not be recruited, as already shown for POC5, leading to the
423 observed futile cycle of centriole formation and disintegration (Wang et al., 2017). It
424 would therefore be interesting to study the presence of WDR90 in these null mutants
425 as well as the other components of the inner scaffold in the future.

426 Our work also showed that POC16 and WDR90 depletion affects centriole
427 length both in *Chlamydomonas reinhardtii* and human cells. While we observed shorter
428 centrioles in *poc16m504* mutants and the opposite, longer centrioles, in WDR90-
429 depleted cells, these results emphasize the role of POC16/WDR90 in overall centriole
430 length regulation and suggest an unexpected role of the inner scaffold structure in
431 centriole length control. The observed discrepancy between the two phenotypes could
432 arise from species differences or from the fact that we analyzed a mutant (truncated
433 protein) in the case of *Chlamydomonas reinhardtii* POC16 versus an RNAi-mediated
434 depletion in the case of human WDR90. Regardless, it would be of great interest to
435 understand if and how the absence of the inner scaffold can affect the length of the
436 centriole without affecting distal markers such as CP110, which remains unchanged in
437 our experiments. It is very likely that the concomitant elongation of the centriole with
438 the appearance of inner scaffold components in G2 can act on the final length of this
439 organelle.

440 Given the importance of centriole integrity in enabling the proper execution of
441 several diverse cellular processes, our work provides new fundamental insights into the
442 architecture of the centriole, establishing a structural basis for centriole stability and the
443 severe phenotypes that arise when lost.

444

445 **Acknowledgments**

We thank Michel Bornens, Eloise Lequoy-Bertiaux and Nikolai Klena for critical reading of the manuscript. We thank Dr. Kanh Huy Bui for sharing his cryo-EM map EMD-20858. We thank the BioImaging Center and PFMU at Unige. We thank Juliette Azimzadeh for sharing the construct GFP-WDR90-FL. We thank the PhD Booster Team of the University of Geneva attributed to E.S. This work is supported by the Swiss National Science Foundation (SNSF) PP00P3_157517 (to P.G.) and 31003A_166608 (to M.O.S.), and by the European research Council ERC ACCENT StG 715289 attributed to Paul Guichard.

Author contributions

E.S. performed and analyzed all the experiments of the paper except for Figure 2C-D. V.H. and Pa.G. conceived, supervised and designed the project. M.O.S. supervised the biochemical microtubule/tubulin-binding experiments. V.H., Pa.G. and E.S. wrote the manuscript with the input from all authors. D.G. and M.L. contributed to U-ExM experiments. C.Z., and N.O. expressed and purified the recombinant proteins used in this study, performed the experiments presented in Figure 2C-D and generated Figure S1A, B. V.O. (together with N. O.) worked on the POC16 model prediction (Figure S2). S.B. provided technical support for the entire study. M.L.G. provided cryo-EM maps and helped with U-ExM data analysis. F.K. and A-M.T. provided expertise and help for the work performed in *Paramecium tetraurelia* (Figure S1C).

Declaration of Interests

The authors declare no competing interests.

Figure legends

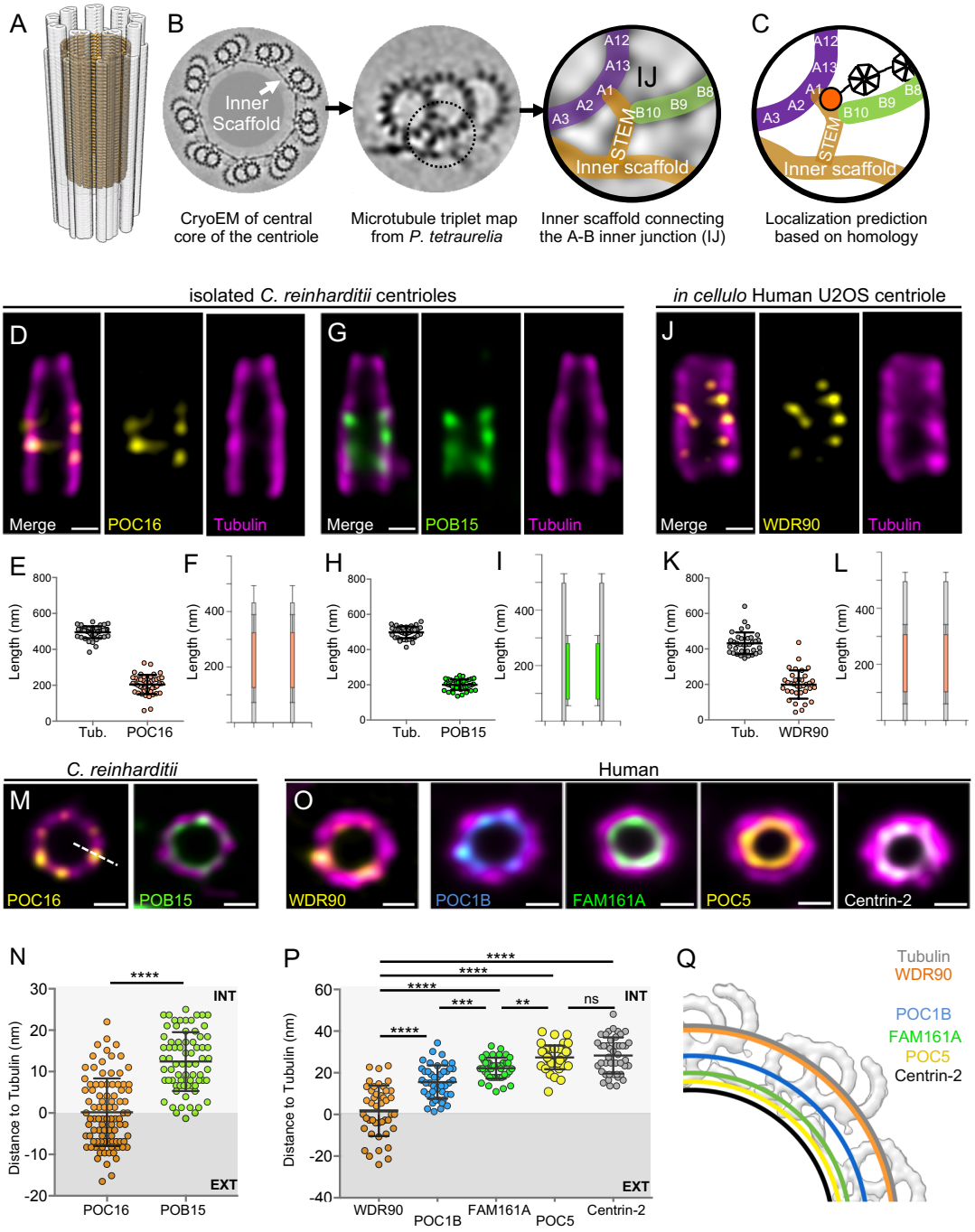

Figure 1. POC16/WDR90 is a conserved central core microtubule wall component. (A) 3D representation of a centriole highlighting the centriolar microtubule wall in light grey and the inner scaffold in yellow. (B) Cryo-EM image of the central core of *Paramecium tetraurelia* centrioles from which a microtubule triplet map has been generated (Le Guennec et al., 2020). Schematic representation of the inner junction (IJ) between A- and B-microtubules connecting the inner scaffold. (C) Schematic

478 localization of POC16/WDR90 proteins within the IJ based on its homology to FAP20.
479 Purple: A-microtubule, green: B microtubule, yellow: inner scaffold and stem, orange:
480 DUF667 domain positioned at the IJ. (D) Isolated U-ExM expanded *Chlamydomonas*
481 centriole stained for POC16 (yellow) and tubulin (magenta), lateral view. Scale bar:
482 100nm. (E) Respective lengths of tubulin and POC16 based on D. Average +/- SD:
483 Tubulin: 495nm +/- 33, POC16: 204nm +/- 53, n=46 centrioles from 3 independent
484 experiments. (F) POC16 length coverage and positioning: 41% +/- 11, n=46 centrioles
485 from 3 independent experiments. (G) Isolated U-ExM expanded *Chlamydomonas*
486 centriole stained for POB15 (green) and tubulin (magenta), lateral view. (H) Respective
487 length of tubulin and POB15 based on G. Average +/- SD: tubulin= 497nm +/- 33,
488 POB15= 200nm +/- 30, n=39 centrioles from 3 independent experiments. (I) POB15
489 length coverage and positioning: 40% +/- 6, n=39 centrioles from 3 independent
490 experiments. (J) *In cellulo* U-ExM expanded human U2OS centriole stained for
491 WDR90 (yellow) and tubulin (magenta), lateral views. (K) Respective lengths of
492 tubulin and WDR90 based on J. Average +/- SD: Tubulin: 432nm +/- 62, WDR90:
493 200nm +/- 80, n=35 from 3 independent experiments. (L) WDR90 length coverage and
494 positioning: 46% +/- 17, n=35 from 3 independent experiments. (M) Isolated U-ExM
495 expanded *Chlamydomonas* centriole stained for tubulin (magenta) and POC16 (yellow)
496 or POB15 (green), top view. Scale bar: 100nm. (N) Distance between the maximal
497 intensity of tubulin and the maximal intensity of POC16 (orange) or POB15 (green)
498 based on M. Average +/- SD: POC16= 0nm +/- 8, POB15= 12nm +/- 7. n>75
499 measurements/condition from 30 centrioles from 3 independent experiments. EXT:
500 exterior or the centriole, INT: interior. (O) *In cellulo* U-ExM expanded human U2OS
501 centriole stained for WDR90 (yellow) and tubulin (magenta), top views, or for core
502 proteins POC1B (blue), FAM161A (green), POC5 (yellow) or Centrin-2 (white). Data

503 set from (Le Guennec et al., 2020). Scale bare: 100nm. (P) Distance between the
504 maximal intensity of tubulin and the maximal intensity of WDR90 (orange) or POC1B
505 (blue), FAM161A (green), POC5 (yellow) or Centrin-2 (grey) based on O. Average +/-
506 SD: WDR90= 2nm +/- 12, POC1B= 15nm+/- 8, FAM161A= 22nm+/-5, POC5= 27nm
507 +/- 6 and Centrin-2= 28nm+/-9. n=45 measurements/condition from 15 to 30 centrioles
508 from 3 independent experiments. Statistics by one-was ANOVA followed by Holm
509 Sidak (Q) Position of WDR90 relative to the four inner scaffold components placed on
510 the cryo-EM map of the *Paramecium* central core region (top view) (adapted from (Le
511 Guennec et al., 2020)).
512

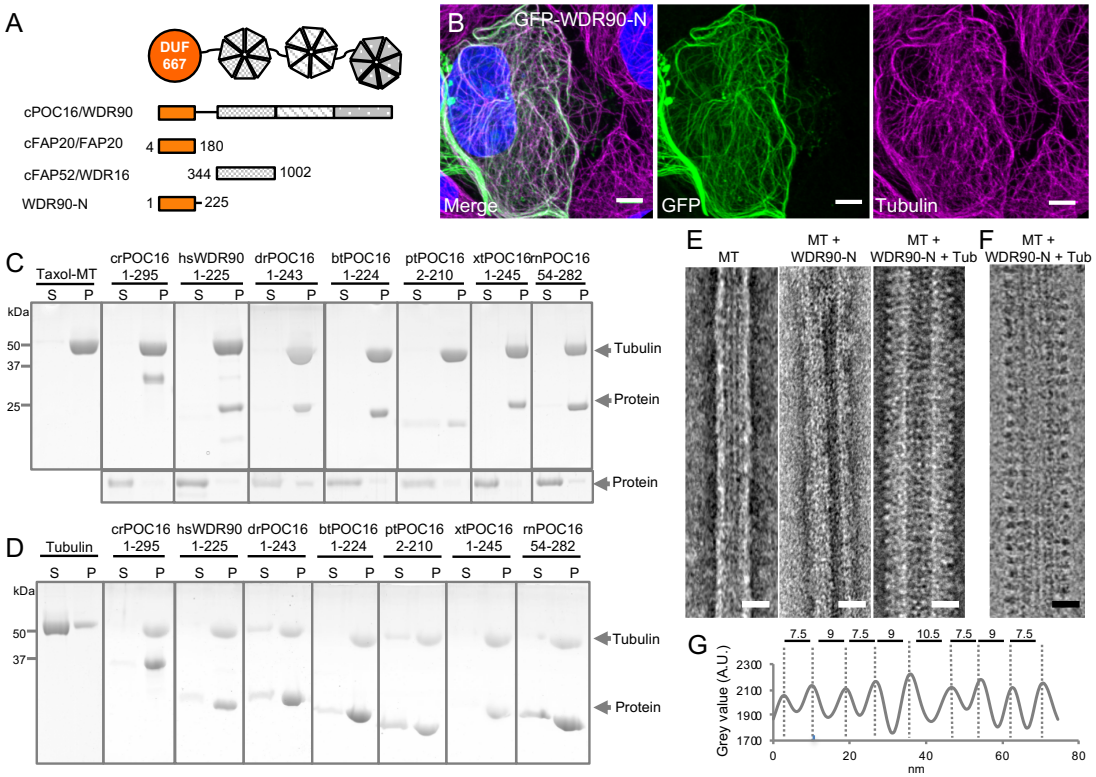

Figure 2. WDR90/POC16-DUF667 directly binds both microtubules and tubulin. (See also Figures S1-S3).

(A) Schematic of WDR90/POC16 conservation and homologous domains with the *Chlamydomonas* cilia proteins FAP20 and FAP52/WDR16. DUF667 domain is in orange and WD40 repeats are in grey. (B) Human U2OS cells transiently overexpressing GFP-WDR90-N (1-225) stained for GFP (green) and tubulin (magenta). Scale bar: 5µm. (C and D) Coomassie-stained SDS-PAGE of pelleting assays performed *in vitro* with taxol-stabilized microtubules (C), and free tubulin (D), in the presence of different recombinant POC16/WDR90-DUF667 protein orthologs (related to Figure S1A, B). The solubility of proteins alone was assessed in parallel to the microtubule-pelleting assay. All tested proteins were soluble under the tested condition (bottom panel). (E) Electron micrographs of negatively stained taxol-stabilized microtubules alone (MT) or subsequently incubated with recombinant WDR90-N (1-

528 225) alone (MT + WDR90-N) or in combination with tubulin (MT + WDR90-N + Tub).
529 Scale bar: 25nm (F) Cryo-electron micrograph of taxol-stabilized microtubules
530 subsequently incubated with recombinant WDR90-N (1-225) and tubulin. Scale bar:
531 25nm (G) Periodicity of complexed WDR90-N (1-225)-tubulin oligomers bound to the
532 microtubule shown in (F).
533

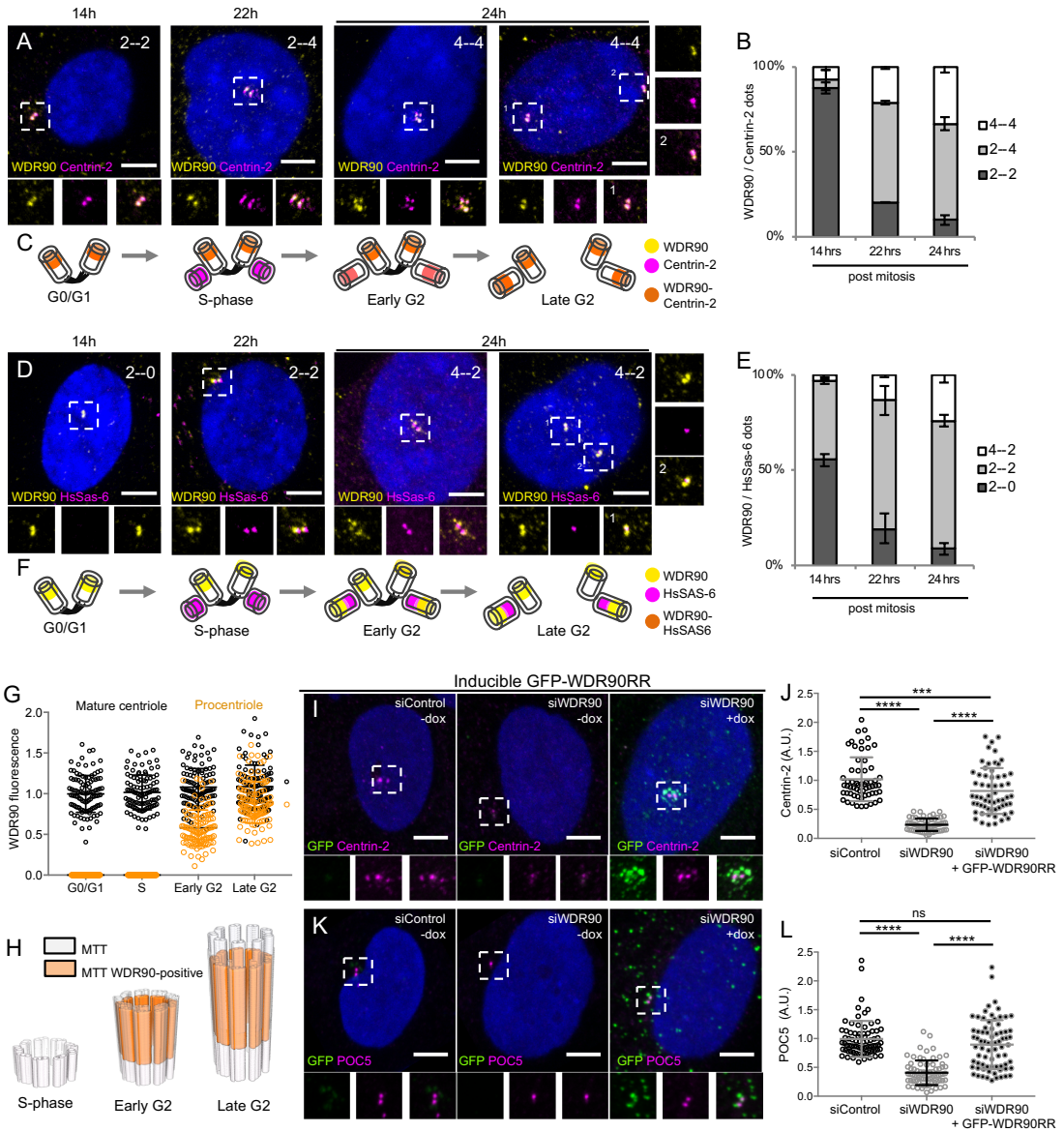

Figure 3. WDR90 is recruited in G2 and is important for inner scaffold components recruitment to centrioles (See also Figures S4 and S5).

(A) Human RPE1 p53- cells synchronized by mitotic shake-off, fixed at different time points for different cell-cycle stages (related to Fig S4A, B) and stained with WDR90 (yellow) and Centrin-2 (magenta). DNA is in blue. Dotted white squares correspond to insets. Numbers on the top right indicate respectively WDR90 and Centrin-2 numbers of dots. Scale bar: 5µm. (B) Percentage of cells with the following numbers of WDR90/Centrin-2 dots based on A, n=300 cells/condition from 3 independent experiments. Average +/- SD: Refer to **Table 2**. (C) Model for WDR90 and Centrin-2

544 incorporation during centriole biogenesis based on A. (D) Human RPE1 p53- cells
545 synchronized by mitotic shake-off, fixed at different time points for different cell-cycle
546 stages and stained with WDR90 and HsSAS-6. (E) Percentage of cells with the
547 following numbers of WDR90 and HsSAS-6 based on D, n=300 cells/condition from
548 3 independent experiments. Average +/- SD: refer to **Table 3**. (F) Model for WDR90
549 and HsSAS-6 incorporation during centriole biogenesis based on D. (G) WDR90
550 fluorescence intensity at centrioles according to cell cycle progression, n=45
551 cells/condition from 3 independent experiments. Black fill represents WDR90 at
552 mature centrioles, orange fill represents WDR90 at procentrioles. (H) Schematic
553 representation of WDR90 incorporation during centriole biogenesis according to cell
554 cycle progression based on G. (I, K) Human U2OS GFP-WDR90 RNAi-resistant
555 version (GFP-WDR90RR) inducible stable cell line treated with control or *wdr90*
556 siRNA and stained for either GFP and Centrin-2 (I) or GFP and POC5 (K) Scale bar:
557 5µm. Dotted white squares indicate insets. - and + dox indicates induction of GFP-
558 WDR90RR expression. (J) Centrosomal Centrin-2 fluorescence intensity based on I,
559 n= 60 cells/condition from 3 independent experiments. Average +/- SEM (A.U.):
560 Control – dox= 1.02 +/- 0.05, siWDR90 – dox= 0.23+/- 0.01, siWDR90 + dox= 0.82
561 +/- 0.01. Statistical significance assessed by one-way ANOVA. (L) Centrosomal POC5
562 fluorescence intensity based on K, n= 75 cells/condition from 3 independent
563 experiments. Average +/- SEM (A.U.): Control – dox= 0.99 +/- 0.04, siWDR90 – dox=
564 0.41+/- 0.02, siWDR90 + dox= 0.89 +/- 0.05. Statistical significance assessed by one-
565 way ANOVA.
566

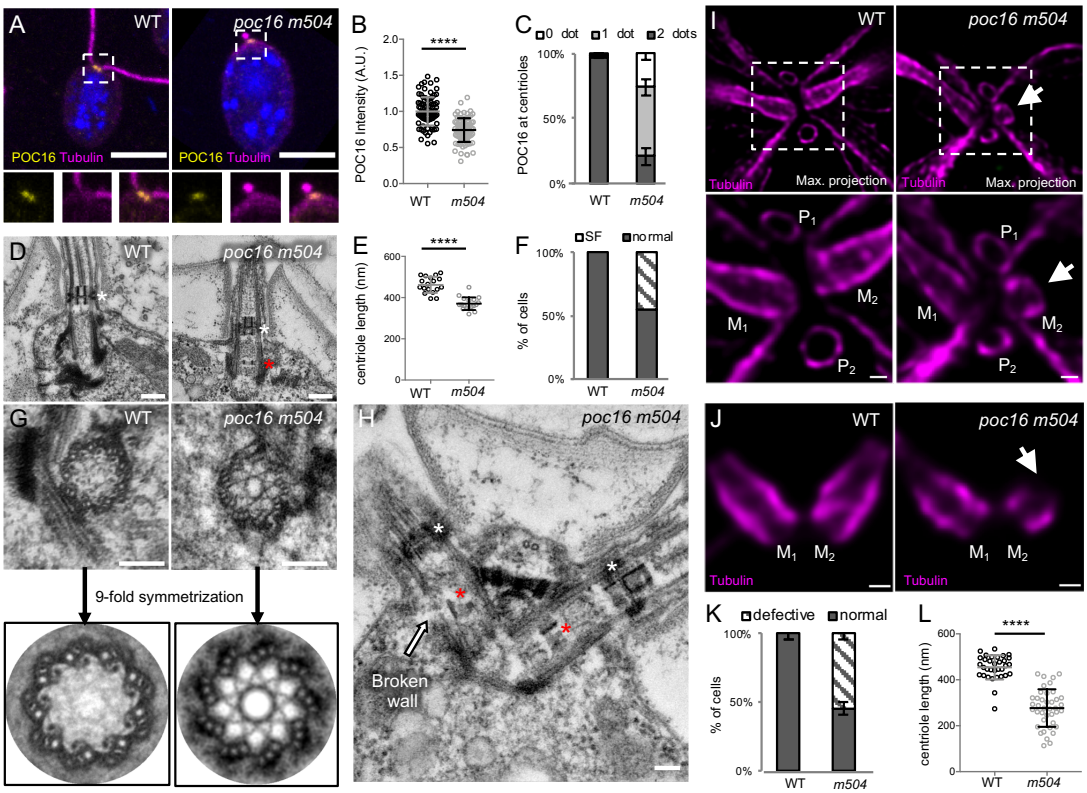

Figure 4. POC16 mutant lacks the inner scaffold (See also Figure S6).

(A) Confocal image of *Chlamydomonas* wild-type (WT) and *poc16 m504* mutant stained for tubulin (magenta) and POC16 (yellow), DNA is in blue. Dotted squares correspond to insets. Scale bar: 5µm. (B) POC16 fluorescence intensity based on A, n=90 cells/condition from 3 independent experiments. Average +/- SD: WT: 1+/- 0.2 (A.U.), *poc16m504*: 0.74 +/- 0.2 (A.U.) Normality assessed by Pearson test, Welch T test p< 0.0001. (C) Percentage of cells displaying two, one or no POC16 dots per cell, n=300 cells/condition from 3 independent experiments. Average +/- SD: WT 2 dots: 97% +/- 0.5, 1 dot: 1.3% +/- 1.5, no dot: 1.3% +/- 1.4; *poc16 m504* 2 dots: 20.1% +/- 6.4, 1 dot: 52% +/- 6.1, no dot: 25.2% +/- 4.5. (D) Electron micrograph of *Chlamydomonas* WT and *poc16 m504* sections revealing the presence of ectopic stellate fibers (SF, white star: normal position in the transition zone; red star: ectopic localization of SF within the central core region of centrioles) inside the lumen of *poc16 m504* centrioles. Scale bar: 250nm (E) Centriole length in WT and *poc16m504* cells,

582 18 centrioles analyzed in each condition. Average +/- SD: WT= 462 +/- 9nm,
583 *poc16m504*= 371 +/- 7nm. Normality assessed by Pearson test, Welch T test p< 0.0001.
584 (F) Percentage of centrioles with ectopic stellate fibers (SF) in WT (0%) and *poc16*
585 *m504* (46%), 18 centrioles analyzed in each condition. (G) Electron micrographs of
586 transversal section of *Chlamydomonas* WT (left) and *poc16 m504* (right) centrioles (top
587 panel) and their corresponding circularized and symmetrized version (bottom panel).
588 Top views circularization and symmetrization were performed using CentrioleJ. Scale
589 bar: 200nm (H) *poc16 m504* mutant displaying a broken centriolar microtubule wall
590 (white arrow). Note the SF in the transition zone (white star) as well as the ectopic SF
591 (red star) within the central core region of *poc16m504* centrioles. Scale bar: 200nm (I)
592 *In cellulo Chlamydomonas* WT or *poc16m504* centrioles/flagella expanded using U-
593 ExM and stained for tubulin (magenta). M stands for mature centriole and P for
594 procentriole. Arrows point to defective mature centrioles. Scale bar: 100nm (J) *In*
595 *cellulo Chlamydomonas* WT or *poc16m504* pair of mature centrioles expanded using
596 U-ExM and stained for tubulin (magenta). Arrows point to defective mature centrioles.
597 Scale bar: 100nm (K) Percentage of cells with abnormal mature centrioles. Average +/-
598 SD: WT 0% +/- 0, *poc16m504*: 55% +/- 5 from 3 independent experiments. (L)
599 Centriolar length based on J, n= 30 centrioles/condition from 3 independent
600 experiments. Average +/- SD: WT 454nm +/- 53, *poc16m504*: 277nm +/- 82. Mann-
601 Whitney test p< 0.0001.
602

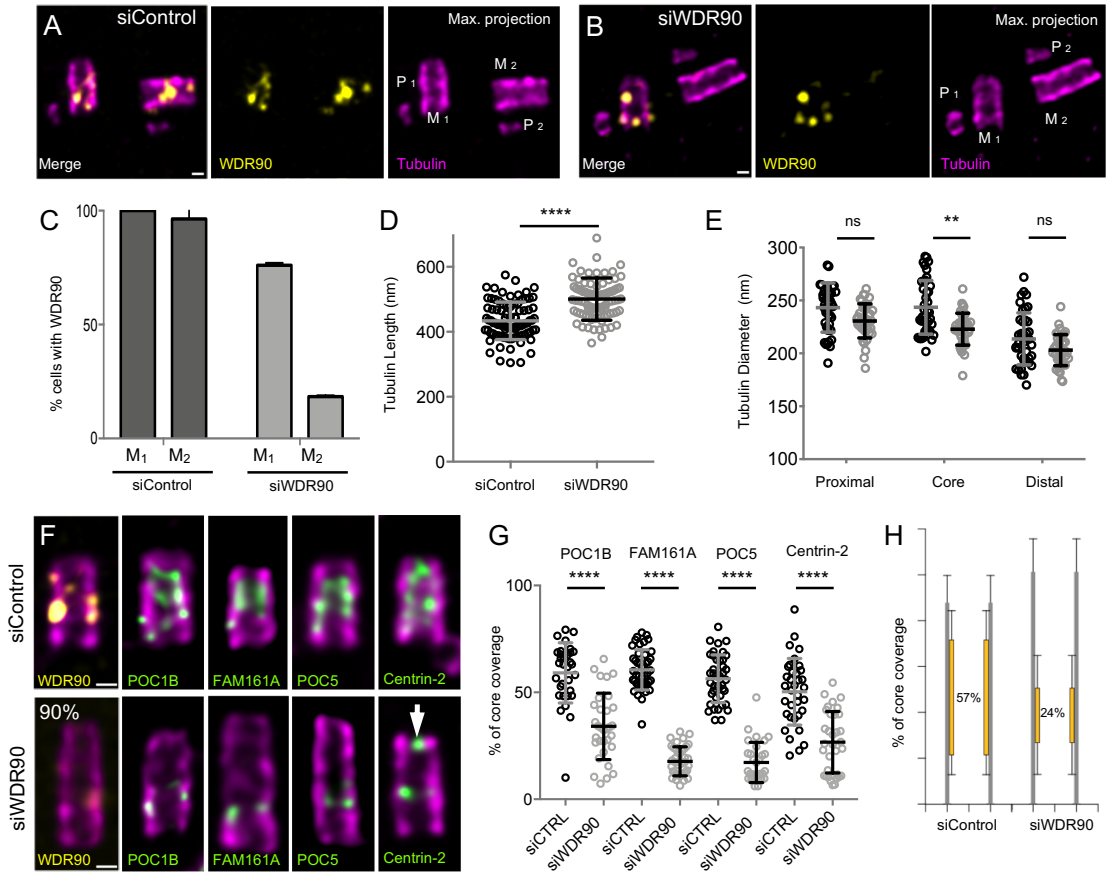

Figure 5. WDR90 is crucial for inner scaffold components localization (see also Figure S7).

(A, B) *In cellulo* U-ExM expanded centrioles from S-phase U2OS treated with either scramble (A) or *wdr90* siRNA (B) stained for tubulin (magenta) and WDR90 (yellow). M stands for mature centriole and P for procentriole. Scale bar: 100nm. (C) Percentage of cells with WDR90 at mature centrioles, n=90 cells/condition from 3 independent experiments Average +/- SD: siControl= M1: 100% +/- 0, M2: 96% +/- 4.7, siWDR90= M1: 76% +/- 1, M2: 18% +/- 0.6. (D) Tubulin length in nm, n=90 centrioles/condition from 3 independent experiments. Average +/- SD: siControl= 434nm +/- 58, siWDR90= 500nm +/- 65. Mann-Whitney p<0.0001. (E) Tubulin diameter measured in the proximal, central core and distal regions of expanded centrioles in siControl (black circles) and *wdr90* siRNA (siWDR90, grey circles). n= 42 and 43 centrioles for siControl and siWDR90 respectively from 2 independent experiments. Averages +/-

617 SD: refer to **Table 4**. Statistical significance assessed by one-way ANOVA. (F) *In*
618 *cellulo* U-ExM expanded U2OS centrioles treated with either scramble or *wdr90*
619 siRNA stained for tubulin (magenta) and WDR90 (yellow) or POC1B, FAM161A,
620 POC5 or Centrin-2 (inner scaffold components: green). Scale bar: 100nm. (G) Inner
621 scaffold protein length, n>30 centrioles/condition from 3 independent experiments.
622 Average +/- SD: refer to **Table 5**. Statistical significance assessed by one-way ANOVA.
623 (H) Average core length coverage. Average +/- SD: siControl= 57% +/- 13; siWDR90=
624 24% +/- 14.
625
626

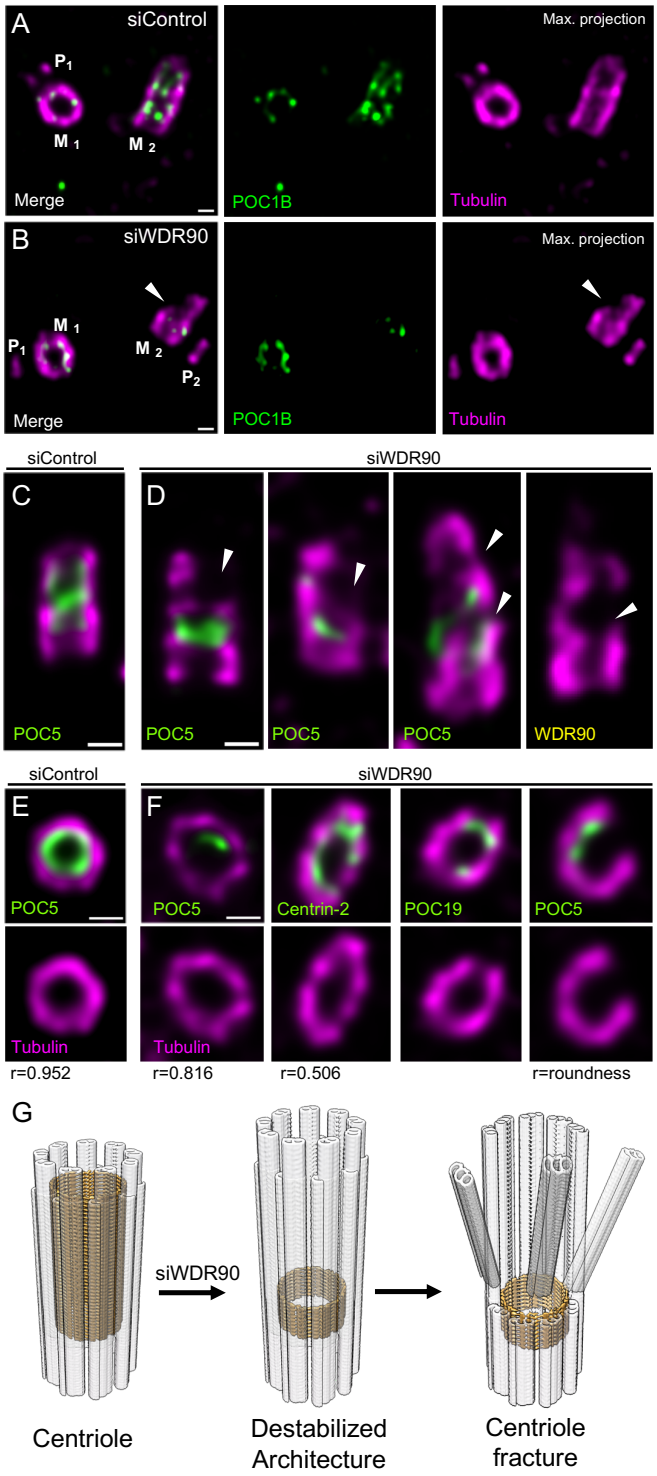

Figure 6. WDR90 is important for centriole architecture integrity (see also Figure S7, Videos 1 and 2).

(A, B) *In cellulo* U-ExM expanded centrioles from S-phase U2OS cells treated with scramble (A) or *wdr90* siRNA (B), stained for tubulin (magenta) and POC1B (green).

632 White arrowhead: broken microtubule wall of the mature centriole. P: procentriole, M:
633 mature centriole. Scale bars: 100nm. (C, D) *In cellulo* U-ExM expanded centrioles from
634 U2OS cells treated with scramble (C) or *wdr90* siRNA (D), stained for tubulin
635 (magenta) and inner scaffold proteins (green, the specific inner core proteins used for
636 each example is written in each panel), displaying microtubule wall fractures (white
637 arrowheads), lateral view. (E, F) Top views of U-ExM expanded centrioles from U2OS
638 cells treated with scramble. Scale bars: 100nm. (E) or *wdr90* siRNA (F) stained as
639 specified above. Note the loss of roundness of centrioles treated with *wdr90* siRNA.
640 (G) Proposed model of WDR90 function holding microtubule triplets in the central core
641 region of centrioles.
642

Supplementary Figure legends

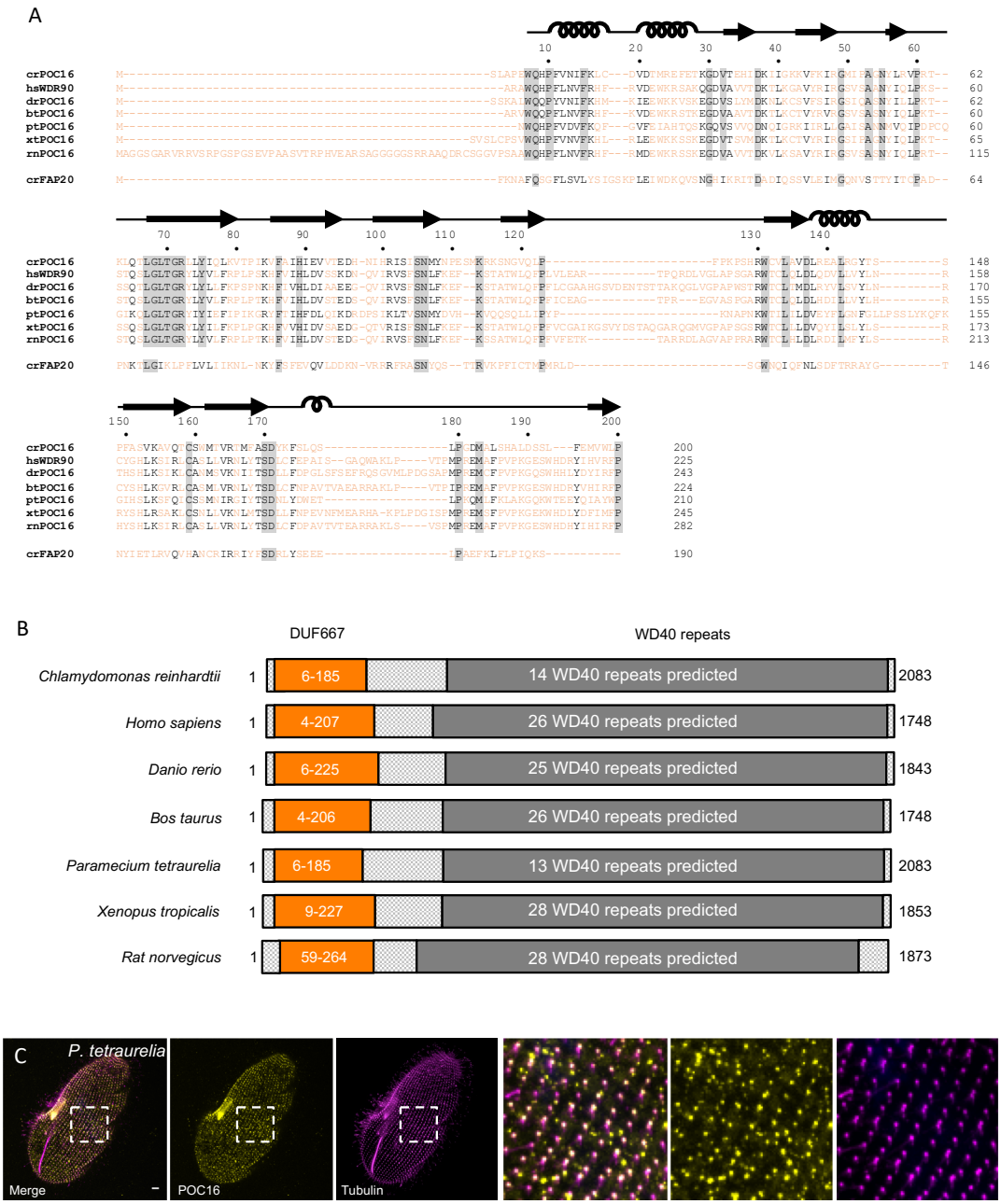

Figure S1. POC16 conservation across species.

(A) POC16 orthologs DUF667 domain amino acids sequence alignment from 7 different species: *Chlamydomonas reinhardtii* crPOC16(1-200); *homo sapiens* hsWDR90(1-225), *Danio rerio* drPOC16(1-243), *Bovine taurus* btPOC16(1-224), *Paramecium tetraurelia* ptPOC16(1-210), *Xenopus tropicalis* xtPOC16(1-245) and *Rat*

651 *norvegicus* rtPOC16(1-282). Note also below the alignment with *Chlamydomonas*
652 *reinhardtii* crFAP20. The secondary structures α-helices and β-strand are indicated on
653 top of the amino acid sequences. (B) POC16 orthologs domain mapping and
654 conservation. Orange: DUF667 domain. Dark grey: WD40 repeats. (C) *Paramecium*
655 *tetraurelia* cell fixed and stained for ptPOC16 (yellow) and tubulin (1D5) (magenta),
656 showing that ptPOC16 is a centriolar component. Scale bare: 10μm .
657

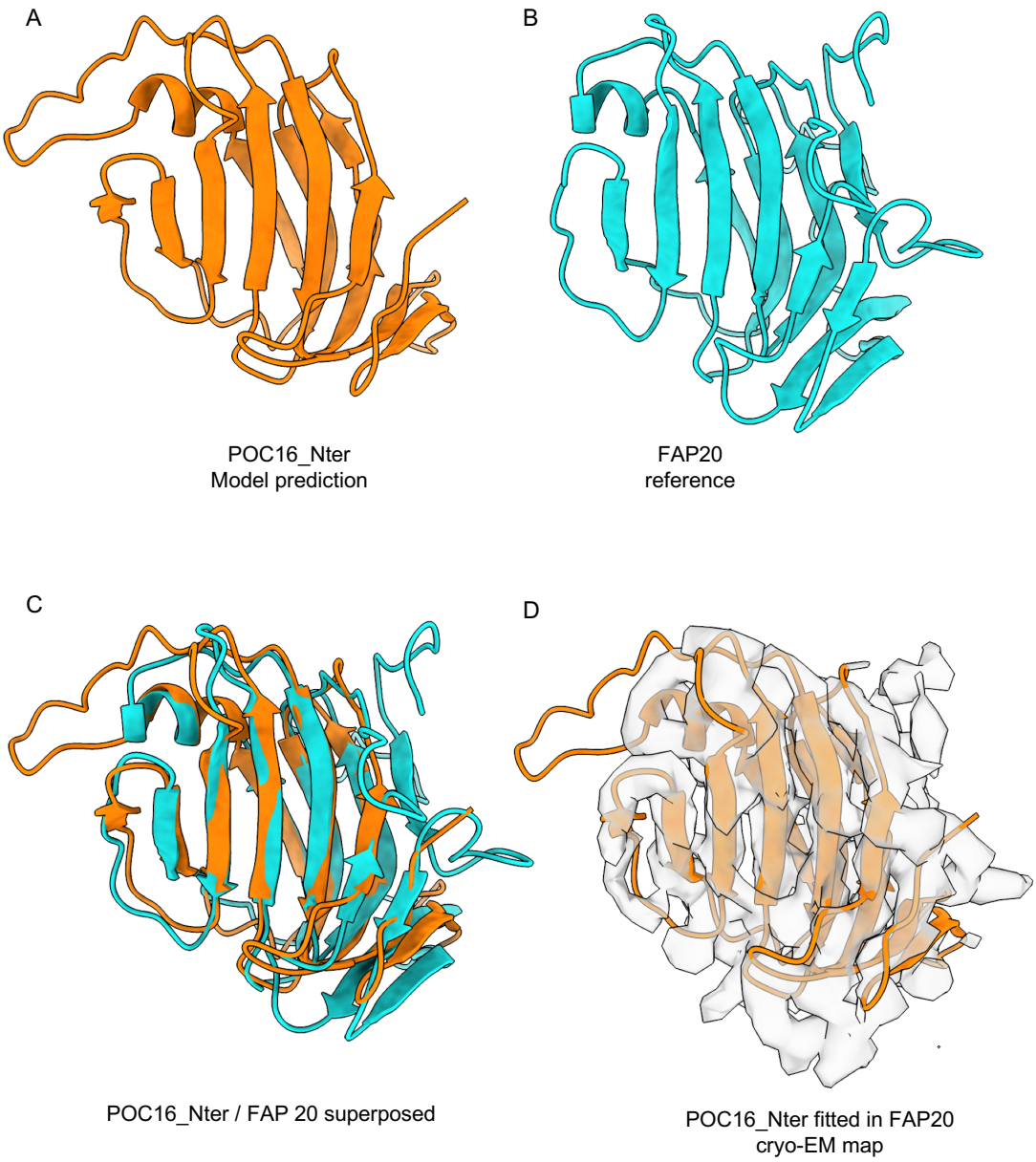

Figure S2. Model prediction of POC16 Nter.

(A) POC16 3D model and (B) FAP20 reference structure model (Khalifa et al., 2019). (C) Fitting of POC16 against FAP20 yielding a RMSD value of 1.6 Angs. (D) Fitting of the POC16 model excluding the flexible loops in the FAP20 cryo-EM electron density map.

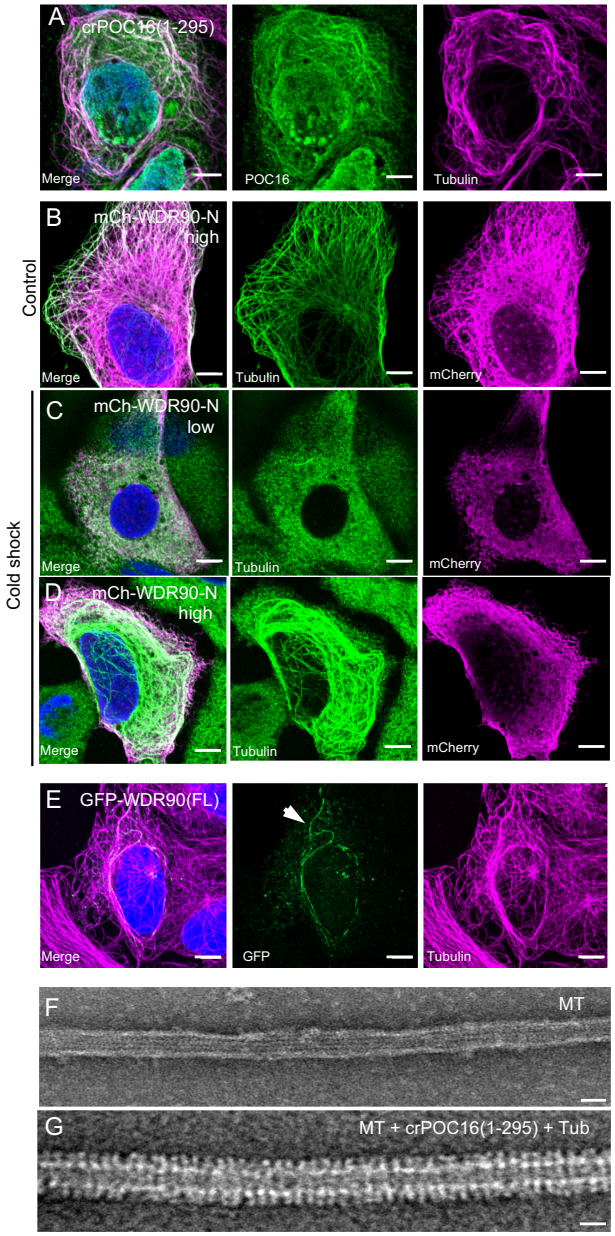

Figure S3. POC16 and WDR90 bind microtubules.

(A) Human U2OS cells transiently overexpressing GFP-crPOC16(1-295) stained for POC16 (green) and tubulin (magenta). Scale bars for panels A-E: 5µm. (B) Human U2OS cells transiently overexpressing at high level mCherry-WDR90-N(1-225), fixed in control condition and stained for tubulin (green) and mCherry (magenta). (C) Human U2OS cells transiently overexpressing at low level mCherry-WDR90-N(1-225), fixed after 1h of cold shock treatment and stained for tubulin (green) and mCherry (magenta). (D) Human U2OS cells transiently overexpressing at high level mCherry-WDR90-N(1-

674 225), fixed after 1h of cold shock treatment and stained for tubulin (green) and mCherry
675 (magenta). (E) Human U2OS cells transiently overexpressing GFP-WDR90(FL)
676 stained for GFP (green) and tubulin (magenta). Arrowhead indicates WDR90-
677 decorated microtubules. (F) Electron micrograph of negatively stained *in vitro* taxol-
678 stabilized microtubules. Scale bar: 25nm (G) Electron micrograph of negatively stained
679 *in vitro* taxol-stabilized microtubules incubated with recombinant POC16(1-295) and
680 free tubulin. Scale bar: 25nm.
681

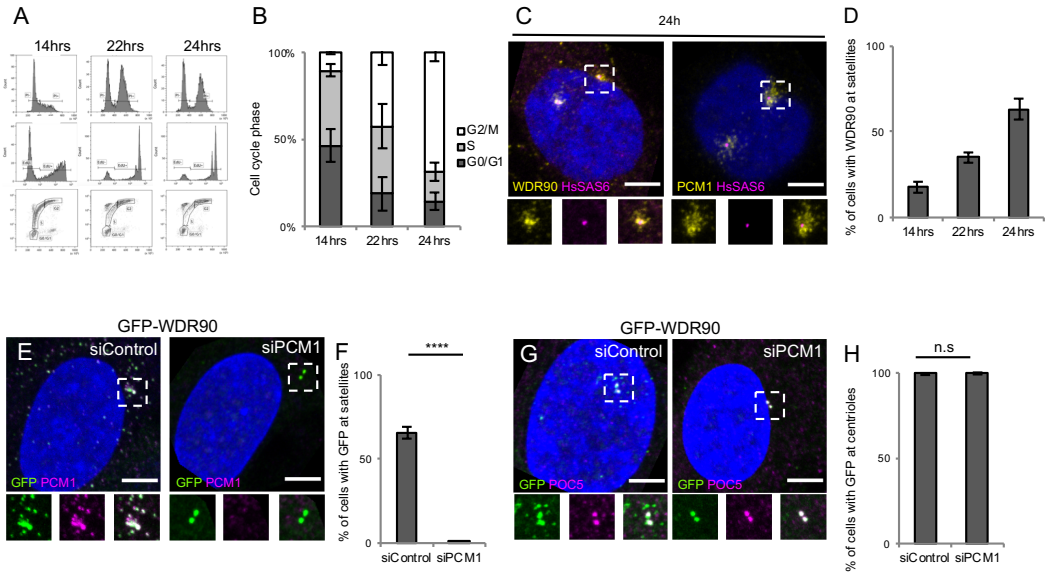

Figure S4. WDR90 is a satellite and centriolar protein.

(A) FACS profiles of RPE1 p53- cells at different time point post mitotic shake-off, plotted based on propidium iodide (PI) and 5-ethynyl-2´-deoxyuridine (EdU) content. Related to Figure 5(A-E). (B) Percentage of cells in G0/G1, S or G2/M phase based on A, n=25000 cells/condition from 3 independent experiments. Average +/- SD: Refers to **Table 6**. (C) Human RPE1 p53- fixed 24 hours post mitosis and stained for WDR90 (yellow) and HsSAS-6 (magenta) or PCM1 (yellow) and HsSAS-6 (magenta). DNA is in blue. Scale bar: 5µm. Dotted white squares indicate insets. (D) Percentage of cells displaying WDR90 satellite pattern based on C, n=150 cells/condition from 3 independent experiments. Average +/- SD: 14hrs: 18% +/- 3, 22hrs: 35% +/- 3, 24hrs: 63% +/- 6. (E) Human U2OS cells expressing GFP-WDR90 treated with scramble or *pcm1* siRNA and stained for GFP and PCM1. Scale bar: 5µm. Dotted white squares indicate insets (F) Percentage of cells with GFP-WDR90 at satellites based on F, n=300 cells/condition from 3 independent experiments Average +/- SD: siControl: 66% +/- 4, siPCM1: 1% +/- 1. Welch T-test $p<0.0001$. (G) Human U2OS cells expressing GFP-WDR90 treated with scramble or *pcm1* siRNA and stained for GFP and POC5. Scale bar: 5µm. Dotted white squares indicate insets. (H) Percentage of cells with GFP-

700 WDR90 at centrioles based on H, n=300 cells/condition from 3 independent
701 experiments Average +/- SD: siControl: 99% +/- 1, siPCM1: 100% +/- 1. Welch T-test
702 p=0.5185.
703

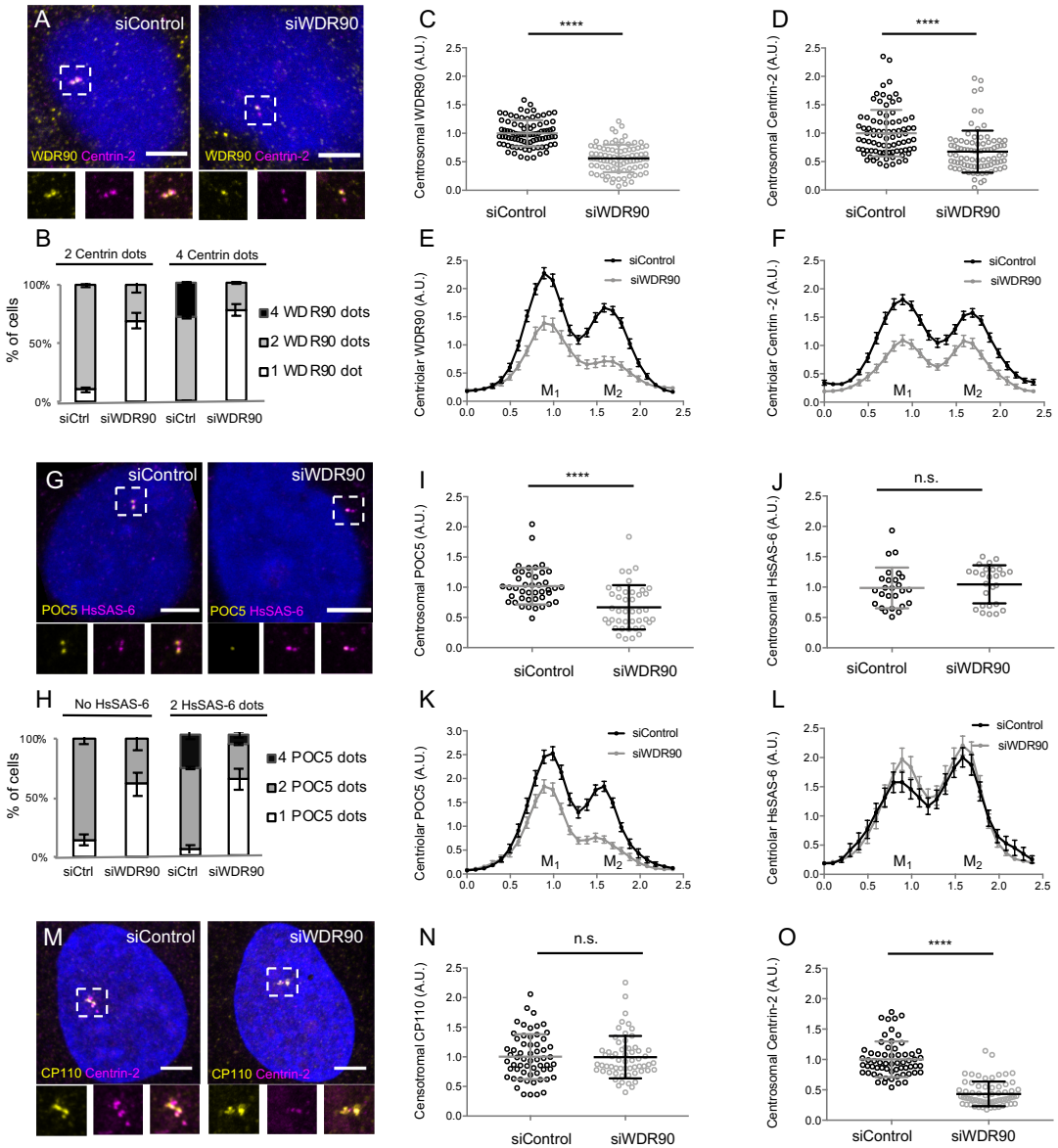

Figure S5. Depletion of WDR90 impairs Centrin-2 and POC5 localization at centrioles.

(A) Human U2OS cell treated with either scramble or *wdr90* siRNA and stained for WDR90 (yellow) and Centrin-2 (magenta). DNA is in blue. Dotted white squares indicate insets. Scale bar: 5µm. (B) Percentage of cells with the following number of WDR90 dots according to the number of Centrin-2 dots per cell based on A, n=150 cells/condition from 3 independent experiments. Average +/- SD: Refer to **Table 7** (C) WDR90 centrosomal intensity based on A, n=90 cells/condition from 3 independent experiments. Average +/- SD: siControl: 1 +/- 0.2 (A.U.), siWDR90: 0.56 +/- 0.2 (A.U.).

714 Normality assessed by Pearson test, Welch T-test p<0.001. (D) Centrin-2 centrosomal
715 intensity based on A, n=90 cells/condition from 3 independent experiments. Average
716 +/- SD: siControl 1 +/- 0.4 (A.U.), siWDR90: 0.68 +/- 0.4 (A.U). Mann-Whitney
717 p<0.001. (E) Plot profiles of WDR90 centriolar intensity based on A, n=90
718 cell/condition from 3 independent experiments. M_1 and M_2 respectively refer to each
719 mature centriole within pairs (F) Plot profiles of Centrin-2 centriolar intensity based on
720 A, n=90 cells/condition from 3 independent experiments. (G) Human U2OS cell treated
721 with either scramble or *wdr90* and stained for POC5 (yellow) and HsSAS6 (magenta).
722 DNA is in blue. Dotted white squares indicate insets. Scale bar: 5µm. (H) Percentage
723 of cells with the following numbers of POC5 dots according to the number of HsSAS-
724 6 dots per cell based on G, n=150 cells/condition from 3 independent experiments.
725 Average +/- SD: Refer to **Table 8** (I) POC5 centrosomal intensity based on G, n=45
726 cells/condition from 3 independent experiments. Average +/- SD: siControl 1 +/-
727 0.3(A.U.), siWDR90: 0.67 +/- 0.4(A.U). Mann-Whitney p<0.001. (J) HsSAS-6
728 centrosomal intensity based on G, n=30 cells/condition from 3 independent
729 experiments. Average +/- SD: siControl 0.99 +/- 0.3 (A.U.), siWDR90: 1 +/- 0.3 (A.U).
730 Mann-Whitney p=0.2551. (K) Plot profiles of POC5 centriolar intensity based on G,
731 n=45 cells/condition from 3 independent experiments. (L) Plot profiles of HsSAS-6
732 centriolar intensity based on G, n=30 cells/condition from 3 independent experiments.
733 (M) Human U2OS cell treated with either scramble or *wdr90* siRNA and stained for
734 CP110 (yellow) and Centrin-2 (magenta). DNA is in blue. Dotted white squares
735 indicate insets. Scale bar: 5µm. (N) CP110 centrosomal intensity based on M, n=60
736 cells/condition from 3 independent experiments. Average +/- SD: siControl 1 +/- 0.4
737 (A.U.), siWDR90: 0.99 +/- 0.4 (A.U). Mann-Whitney p=0.7756. (O) Centrin-2
738 centrosomal intensity based on M, n=55 cells/condition from 3 independent

739 experiments. Average +/- SD: siControl 1 +/- 0.3 (A.U.), siWDR90: 0.4 +/- 0.2 (A.U).

740 Mann-Whitney $p<0.0001$. Note that Centrin-2 intensity served as an internal control for

741 the efficient depletion of WDR90 by siRNA in this experiment.

742

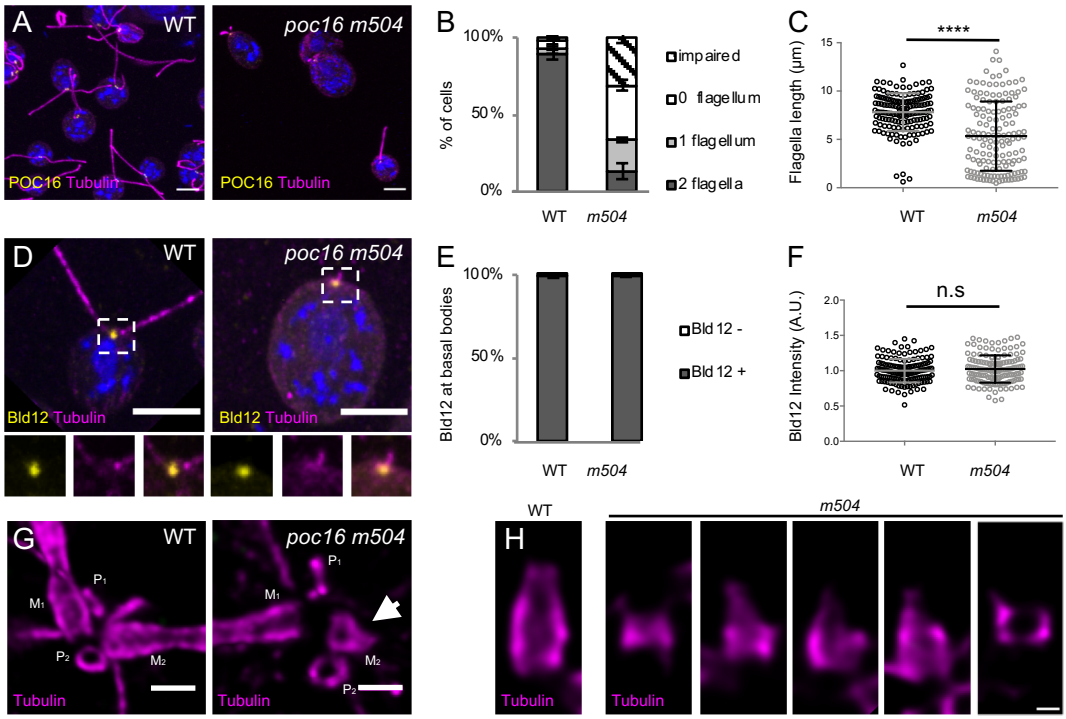

743

744 **Figure S6. POC16 is important for flagella assembly and proper centriolar**

745 **structure.**

746 (A) Confocal image of *Chlamydomonas* WT and *poc16 m504* cells stained with tubulin

747 (magenta) and POC16 (yellow). Scale bar: 5µm (B) Percentage of cells with 0, 1, 2 or

748 impaired flagella, n=300 cells/condition from 3 independent experiments. Average +/-

749 SD: WT: 2 flagella= 95.5% +/- 4, 1 flagellum= 2.2% +/- 2, no flagellum= 2.3% +/- 2,

750 impaired flagellum= 0% +/- 0; *poc16 m504:* 2 flagella= 13% +/- 5, 1 flagellum= 20%

751 +/- 2, no flagellum: 13% +/- 3, impaired flagellum= 31% +/-3. (C) Flagellar length in

752 µm, n=150 cells/condition from 3 independent experiments. Mann Whitney test

753 p<0.0001. (D) *Chlamydomonas* WT and *poc16 m504*-mutant stained with tubulin

754 (magenta) and Bld12 (yellow). Scale bar: 5µm (E) Percentage of cells positive for

755 Bld12 at centrioles, n=300 cells/condition from 3 independent experiments. Average

756 +/- SD: WT Bld12 positive (Bld12+) 99% +/- 1, *poc16m504*: 99% +/- 1. Normality

757 assessed by Pearson test, Welch T test p< 0.0001. (F) Bld12 fluorescence intensity,

758 n=150 cells/condition from 3 independent experiments. Average +/- SD: WT= 1 +/-

759 0.01 (A.U.), *poc16m504*= 1 +/- 0.02 (A.U.). Normality assessed by Pearson test, Welch
760 T test p=0.0714. (G) *In cellulo Chlamydomonas* WT or *poc16m504* centrioles/flagella
761 U-ExM expanded stained for tubulin (magenta). M stands for mature centriole, P for
762 procentriole. Arrows point to defective mature centriole. Scale bar: 400nm (H) Gallery
763 of *poc16m504* defective short mature centrioles stained with tubulin (magenta)
764 compared to a WT mature centriole (left panel). Scale bar: 100nm.
765

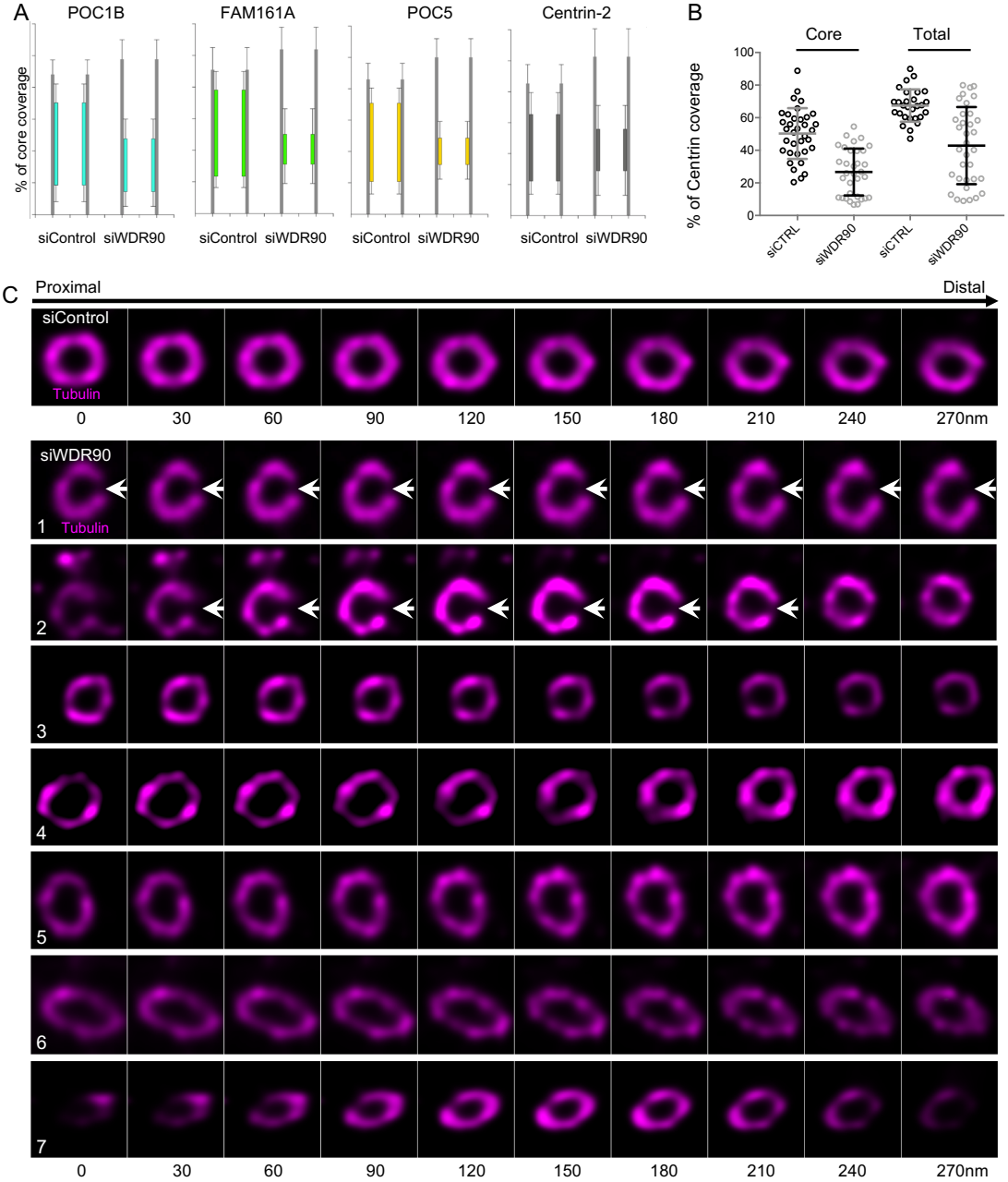

766

767 **Figure S7. WDR90 depletion leads to severe centriolar structure defects.**

768 (A) Inner scaffold protein length based on Figure 5D and 5E, n>30 centrioles/condition

769 from 3 independent experiments. (B) Centrin-2 length based on Figure 5D, measuring

770 inner core or total (core + distal) length. (C) *In cellulo* U-ExM expanded centriole from

771 U2OS cells treated with siRNA targeting scramble genes or *wdr90* stained for tubulin,

772 top views. White arrows indicate centriole fracture. Scale bar: 200nm

773

774

775

776 **Video1**. **U-ExM expanded control centrioles.**

777 Top viewed *in cellulo* U-ExM expanded centriole from U2OS cell treated with

778 scramble siRNA and stained for tubulin (magenta) and POC5 (green). Z-stack acquired

779 every 0.12µm from the proximal to distal end of the centriole.

780

781 **Video2**. **U-ExM expanded centrioles depleted of WDR90.**

782 Top viewed *in cellulo* U-ExM expanded centriole from U2OS cell treated with *wdr90*

783 siRNA and stained for tubulin (magenta) and POC5 (green). Z-stack acquired every

784 0.12µm from the proximal to distal end of the centriole.

785

786

787 **Supplementary Tables**

x value for maximal intensity peak (nm)	Tubulin	Inner scaffold proteins
POC1B	53.99	68.48
FAM161A	51.36	73.75
POC5	46.09	72.43
Centrin-2	47.41	77.70

788 **Table 1:** Tubulin and inner scaffold proteins fluorescence intensity on microtubule
789 triplets from external to internal.
790

	Time		
Percentage of cells	**14hrs**	**22hrs**	**24hrs**
2--0	57 +/- 2	20 +/- 1	10 +/- 3
2--2	38 +/- 4	59 +/- 1	57 +/- 4
4--2	5 +/- 13	21 +/- 15	33 +/- 45

791 **Table 2:** Percentage of cells with the following number of dots/cell respectively for
792 WDR90 and Centrin-2.
793

	Time		
Percentage of cells	**14hrs**	**22hrs**	**24hrs**
2--0	53 +/-3	19 +/- 6	9 +/- 3
2--2	44 +/- 4	67 +/- 1	67 +/- 3
4--2	3 +/- 1	13 +/- 1	24 +/- 4

794 **Table 3:** Percentage of cells with the following number of dots/cell respectively for
795 WDR90 and HsSAS-6.
796

Diameter	siControl	siWDR90
Proximal	243 +/-23 nm	231 +/- 16 nm
Core	244 +/-25 nm	223 +/- 15 nm
Distal	214 +/- 25 nm	203 +/- 15 nm

797 **Table 4:** Diameter at proximal, core and distal region of the centriole

798

Length coverage	siControl	siWDR90
POC1B	59 +/-14 nm	34 +/- 16 nm
FAM161A	61 +/- 9 nm	18 +/- 7 nm
POC5	56 +/- 11 nm	17 +/- 9 nm
Centrin-2	50 +/- 16 nm	27 +/- 14 nm

799 **Table 5:** Inner scaffold proteins length coverage

800

	Time		
Percentage of cells	**14hrs**	**22hrs**	**24hrs**
G0/G1	47 +/- 10	19 +/- 10	14 +/- 5
S	43 +/- 4	39 +/- 13	17 +/- 5
G2/M	10 +/- 1	42 +/- 7	69 +/- 5

801 **Table 6:** Percentage of cells in each phase of the cell cycle according to post-mitotic
802 time point
803

% of cells	**2 Centrin-2 dots**			**4 Centrin-2 dots**		
	0 WDR90	1 WDR90	2 WDR90	1 WDR90	2 WDR90	4 WDR90
siControl	0 +/- 0	10 +/- 2	90 +/- 2	0 +/- 0	71 +/- 1	29 +/- 1
siWDR90	0 +/- 0	69 +/- 7	31 +/- 7	77 +/- 5	23 +/- 5	0 +/- 0

804 **Table 7:** Percentage of cells displaying 0, 1, 2 or 4 dots of WDR90 based on the number
805 of Centrin-2 dots in U2OS cells treated with siRNA targeting scramble genes or *wdr90*
806

% of cells	**0 HsSAS-6 dot**			**2 HsSas-6 dots**		
	0 POC5	1 POC5	2 POC5	1 POC5	2 POC5	4 POC5
siControl	0 +/- 0	14 +/- 5	86 +/- 5	4 +/- 4	68 +/- 6	28 +/- 4
siWDR90	0 +/- 0	61 +/- 10	39 +/- 10	63 +/- 9	29 +/- 11	8 +/- 3

807 **Table 8:** Percentage of cells displaying 0, 1, 2 or 4 dots of POC5 based on the number
808 of HsSas-6 dots in U2OS cells treated with siRNA targeting scramble genes or *wdr90*
809

810

811 **EXPERIMENTAL MODEL AND SUBJECT DETAILS**

812 ***Chlamydomonas reinhardti* strains**

813 *Chlamydomonas* strains control wild-type WT (cMJ030, *Chlamydomonas* Resource
814 Center) as well as *poc16 m504* (LMJ.RY0402.069504, *Chlamydomonas* Resource
815 Center) were described and cultured similarly to Hamel et al, 2017.

816

817 **Human cell lines**

818 Human U2OS and RPE1 p53- cells (gift from Meng-Fu Bryan Tsou) were cultured
819 similarly to Hamel et al, 2017. Cells were grown in DMEM supplemented with
820 GlutaMAX (Life Technology), 10% tetracycline-negative fetal calf serum (life
821 technology), penicillin and streptomycin (100 µg/ml).
822 To generate inducible episomal U2OS:GFP-WDR90RR cell line, U2OS cells were
823 transfected using Lipofectamine 3000 (Life Technology). Transfected cells were
824 selected for 6 days using 1µg/mL puromycin starting day 2 after transfection. Selected
825 cells were amplified and frozen. For further experiments, U2OS:GFP-WDR90 cell line
826 was grown in the medium specified above supplemented with 1µg/mL puromycin.

827

828 **METHOD DETAILS**

829 **Ultrastructure Expansion Microscopy (U-ExM)**

830 The following reagents were used in U-ExM experiments: formaldehyde (FA, 36.5-
831 38%, F8775, SIGMA), acrylamide (AA, 40%, A4058, SIGMA), N,N'-
832 methylenbisacrylamide (BIS, 2%, M1533, SIGMA), sodium acrylate (SA, 97-99%,
833 408220, SIGMA), ammonium persulfate (APS, 17874, ThermoFisher),
834 tetramethylethylendiamine (TEMED, 17919, ThermoFisher), nuclease-free water
835 (AM9937, Ambion-ThermoFisher) and poly-D-Lysine (A3890401, Gibco).

836 Monomer solution (MS) for one gel is composed of 25 µl of SA (stock solution at 38%
837 (w/w) diluted with nuclease-free water), 12.5 µl of AA, 2.5 µl of BIS and 5 µl of 10X
838 phosphate-buffered saline (PBS).
839 For isolated *Chlamydomonas* basal bodies (Klena et al., 2018), U-ExM was performed
840 as previously described (Gambarotto et al., 2019). *In cellulo Chlamydomonas* U-ExM
841 was performed on cells sedimented for 15 min on Poly-D-lysine-coated coverslips.
842 Briefly, coverslips were incubated in 1% AA + 0.7% FA diluted in 1X PBS (1X
843 AA/FA) for 5hrs at 37°C prior to gelation in MS supplemented with TEMED and APS
844 (final concentration of 0.5%) for 1h at 37°C and denaturation for 30min at 95°C.
845 Specifically, gels were stained for 3hrs at 37°C with primary antibodies against tubulin
846 monobody (A345) (1:250 for cells and 1:500 for isolated basal bodies, scFv-F2C,
847 Alpha-tubulin) (Nizak et al., 2003) and POC16 (1:100) (Hamel et al., 2017) or POB15
848 (1:100) (Hamel et al., 2017) diluted in 2% PBS/BSA. Gels were washed 3x10min in
849 PBS with 0.1% Tween 20 (PBST) prior to secondary antibodies incubation for 3hrs at
850 37°C and 3x10min washes in PBST. A second round of expansion was done 3x150mL
851 ddH20 before imaging.
852 Human U2OS cells were grown on 12mm coverslips and processed as previously
853 described (Le Guennec et al., 2020). Briefly, coverslips were incubated for 5 hours in
854 2% AA + 1.4% FA diluted in 1X PBS (2X AA/FA) at 37°C. Denaturation was
855 performed for 1h30 at 95°C and gels were stained as described above. The following
856 primary antibodies were used: tubulin monobodies AA344 (1:250, scFv-S11B, Beta-
857 tubulin) and AA345 (1:250, scFv-F2C, Alpha-tubulin) (Nizak et al., 2003), rabbit
858 polyclonal anti-POC1B (1:250, PA5-24495, ThermoFisher), rabbit polyclonal anti-
859 POC5 (1:250, A303-341A, Bethyl), rabbit polyclonal anti-FAM161A (1:250) (Le
860 Guennec et al., 2020), mouse monoclonal anti-Centrin-2 (1:250, clone 20H5, 04-1624,

861 Merck Millipore), rabbit polyclonal anti-WDR90 (1:250, NovusBio NBP2-31888).
862 Specifically, staining against WDR90 was performed overnight at 37°C.
863
864 The following secondary antibodies were used: goat anti-rabbit Alexa Fluor 488 IgG
865 H+L (1:400, A11008) and goat anti-mouse Alexa Fluor 568 IgG H+L (1:250, A11004)
866 (Invitrogen, ThermoFisher).
867
868 For each gel, a caliper was used to accurately measure its expanded size (Ex_{size} in mm).
869 The gel expansion factor (X factor) was obtained by dividing Ex_{size} by 12mm, which
870 corresponds to the size of the coverslips use for sample seeding.
871 Thus, X factor = Ex_{size} (mm)/12(mm). The table below shows the Ex_{size} and X factor for
872 all the gels used in this study.

Gel	**siControl** **Ex_{size} (X factor)**	**siWDR90** **Ex_{size} (X factor)**
POC1B (n=1)	53 mm (4.42)	52 mm (4.33)
POC1B (n=2)	49 mm (4.08)	50.5 mm (4.21)
POC1B (n=3)	50.5 mm (4.21)	50.5 mm (4.21)
FAM161A (n=1)	50 mm (4.16)	50 mm (4.16)
FAM161A (n=2)	50 mm (4.16)	51 mm (4.25)
FAM161A (n=3)	50 mm (4.16)	50 mm (4.16)
POC5 (n=1)	51 mm (4.25)	50.5 mm (4.21)
POC5 (n=2)	50 mm (4.16)	50 mm (4.16)
POC5 (n=3)	50.5 mm (4.21)	49 mm (4.08)
Centrin-2 (n=1)	50 mm (4.16)	50 mm (4.16)
Centrin-2 (n=2)	50 mm (4.16)	50 mm (4.16)

Centrin-2 (n=3)	49 mm (4.08)	49 mm (4.08)

873

874 Pieces of gels were mounted on 24mm round precision coverslips (1.5H, 0117640,
875 Marienfeld) coated with poly-D-lysine for imaging. Image acquisition was performed
876 on an inverted Leica TCS SP8 microscope using a 63X 1.4NA oil objective with
877 Lightening mode at max resolution, adaptive as 'Strategy" and water as "Mounting
878 medium" to generate deconvolved images. 3D stacks were acquired with 0.12µm z-
879 intervals and an x, y pixel size of 35nm

880

881 **Cloning, and transient overexpression in Human cells**

882 GFP-WDR90-N(1-225)RR and GFP-WDR90(FL)RR were cloned in the Gateway
883 compatible vector pEBTet-eGFP-GW. Previously generated RNAi-resistant WDR90
884 DNA (Hamel et al, 2017) was used as template for PCR amplification. In brief, inserts
885 were first subcloned in pENTR-Age-AGT using the restriction sites AgeI and XbaI.
886 Second, a Gateway reaction was performed to generate the final expression plasmids
887 pEBTet-GFP-WDR90-N(1-225)RR and pEBTer-GFP-WDR90(FL)RR, which were
888 sequenced verified prior to transfection in human cells.

889 For transient expression, U2OS cells were transfected using Lipofectamine 3000 (Life
890 Technology). Protein expression was induced using 1µg/mL doxycycline for 48 hours
891 and cells were processed for immunofluorescence analysis.

892 Cloning of the GFP-WDR90 construct used in Figure 2 was done as follows: Human
893 WDR90 was cloned by nested RT-PCR using total RNAs extracted from human RPE1
894 cells. Three different fragments corresponding to aa. 1-578, 579-1138, 1139-1748 of
895 WDR90 (based on Genebank sequence NP_660337) were amplified and cloned
896 separately using the pCR Blunt II Topo system (Thermo Fisher Scientific). The full

897 coding sequence was then reconstituted in pCR Blunt II by two successive cloning steps
898 using internal *Nru* I and *Sal* I, introduced in the PCR primers and designed in order not
899 to modify WDR90 aa sequence. WDR90 coding sequence was then cloned into a
900 modified pEGFP-C1 vector (Clontech) containing *Asc* I and *Pac* I restriction sites.
901
902 **Immunofluorescence in Human cells**
903 Cells grown on a 15 mm glass coverslips (Menzel Glaser) were pre-extracted for 15sec
904 in PBS supplemented with 0.5% triton prior to iced-cold methanol fixation for 7min.
905 Cells were washed in PBS then incubated in 1% bovine serum albumin (BSA) in PBS-
906 T with primary antibodies against WDR90 (1:250), Centrin-2 (1:500), HsSAS-6
907 (1:100), PCM1 (1:500), CP110 (1:500), GFP (1:500), mCherry (1:500) or tubulin
908 (1:500). Coverslips were washed in PBS for 30min prior to incubation with secondary
909 antibodies (1:1000) for 1 hour at room temperature, washed again for 30min in PBS
910 and mounted in DAPCO mounting medium containing DAPI (Abcam).
911 Imaging was performed on a Zeiss LSM700 confocal microscope with a PlanApo 63x
912 oil immersion objective (NA 1.4) and optical sections were acquired every 0.33 m,
913 then projected together using ImageJ.
914
915 **Cloning and protein purification**
916 The constructs encompassing the predicted DUF667 domain of crPOC16 (Uniprot:
917 A8JAN3), hsWDR90 (Uniprot: Q96KV7), drPOC16 (Uniprot: F1RA29), btPOC16
918 (Uniref: UPI000572B175), ptPOC16 (Uniprot: A0DK60),
919 xtPOC16 (Uniref: UPI0008473371) and rnPOC16 (Uniref UPI0008473371) were
920 cloned into a pET based expression vector via Gibson assembly (Gibson et al., 2009).

921 All recombinant proteins contained a N-terminal thioredoxin (TrxA) tag, used to
922 enhance the expression level and the solubility of the target protein, followed by a
923 6xHis tag and a 3C cleavage site.
924 Protein expression was carried out in *E. coli* BL21 (DE3) competent cells grown in LB
925 media at 37°C to OD_{600} = 0.6 and induced for 16h at 20°C with 1mM IPTG. Cells were
926 subsequently resuspended in lysis buffer (50 mM Hepes pH 8, 500 mM NaCl, 10% v/v
927 glycerol, 10 mM imidazole pH 8, 5 mM β-mercaptoethanol) supplemented with DNase
928 I (Sigma), complete EDTA-free protease inhibitor cocktail (Roche) and lysed by
929 sonication. The supernatant was clarified by centrifugation (18000 rpm, 4˚C, 45 min),
930 filtered and loaded onto a HisTrap HP 5 ml column (GE Healthcare). After extensive
931 washes with wash buffer (50 mM Hepes pH 8, 500 mM NaCl, 10% v/v glycerol, 20
932 mM imidazole pH 8, 5 mM β-mercaptoethanol), the bound protein was eluted in the
933 wash buffer supplemented with 400 mM imidazole. For crPOC16, hsWDR90,
934 drPOC16 and xtPOC16, a 10 to 400 mM imidazole gradient was required to
935 successfully detach the protein from the column.
936 The protein-containing fractions were pooled together and dialysed against the lysis
937 buffer at 4˚C for 48 hours in the presence of the 6xHis-3C protease. The tag-free protein
938 was reapplied onto a HisTrap HP 5 ml column (GE Healthcare) to separate the cleaved
939 product from the respective tags and potentially uncleaved protein. The processed
940 proteins were concentrated and further purified by size exclusion chromatography
941 (Superdex-75 16/60, GE Healthcare) in running buffer (20 mM Tris pH 7.5, 150 mM
942 NaCl, 2 mM DTT). Protein were analysed by Coomasie stained SDS-PAGE and the
943 protein-containing fractions were pooled, concentrated and flash-frozen for storage at -
944 80˚C. All protein concentrations were estimated by UV absorbance at 280 nm.
945

946 **Microtubule binding assay**

947 Taxol-stabilized microtubules (MTs) were assembled in BRB80 buffer (80 mM PIPES-
948 KOH pH6.8, 1 mM $MgCl_2$, 1 mM EGTA) from pure bovine brain tubulin at 1 mg/mL
949 (Centro de Investigaciones Biológicas, Madrid, Spain). 50 µL of stabilized MTs were
950 incubated with 20µL of protein at 1 mg/mL for 2 hours at room temperature. After
951 centrifugation on a taxol-glycerol cushion (8'000 rpm, 30°C, 20min) the supernatant
952 and the pellet were analyzed by Coomasie stained SDS-PAGE gels. As a control, MTs
953 alone and each protein alone were processed the same way.

954

955 **Tubulin binding assay**

956 Tubulin at 10 µM was incubated with a slight molar ratio excess of each protein
957 construct (around 15 µM) in MES buffer for 15 min on ice. After centrifugation at
958 13'000 x g at 4°C for 20 min, the supernatant and the pellet were analyzed by Coomasie
959 stained SDS-PAGE.

960

961 ***In vitro* microtubules decoration and imaging**

962 For simple decoration, Taxol-stabilized microtubules were nucleated as described
963 (Schmidt-Cernohorska et al., 2019) and subsequently exposed to recombinant WDR90-
964 N(1-225) in a 1:1 molar ratio for 30min at room temperature. Five µL of protein
965 complexes solution were blotted on Lacey carbon grids and stained with Uranyl Acetate
966 (2%) for 3 then 30 seconds.

967 For double decoration, *in vitro* microtubules were incubated with WDR90-N(1-225) in
968 a 1:1 molar ratio for 5min at room temperature prior to addition of 2X free tubulin for

969 30min at room temperature. Negatively stained grids were prepared as above. Similarly,
970 double decorated microtubules were prepared for cryo-fixation.
971 Electron micrographs were acquired on a Technai 20 electron microscope (FEI
972 Company) and analyzed using ImageJ.
973
974
975 **Mitotic shake off**
976 RPE1 p53- cells were seeded in T300 flasks the day before shake off. Flasks were
977 shaken vigorously to detach mitotic cells collected in medium. Cells were pelleted by
978 centrifugation for 5min at 1000 rpm and suspended in 10nM EdU containing medium
979 prior to seeding in 6 well plates onto 15mm coverslips. Cells were fixed at different
980 time points and processed in parallel for immunofluorescence or FACS analysis.
981
982 **WDR90 depletion using siRNA**
983 U2OS cells were plated onto 15mm coverslips in a 6-well plate and 10nM silencer
984 select pre-designed siRNA s47097 was transfected using Lipofectamine RNAimax
985 (Thermo Fischer Scientific). Medium was changed 4hrs and 48hrs post-transfection and
986 cells were analyzed 96hrs post-transfection.
987 In U2OS:GFP-WDR90(FL-RR) stable cell line, RNA-resistant protein expression was
988 induced constantly for 96hrs using 1µg/mL doxycycline.
989
990 **Immunofluorescence on *Chlamydomonas reinhardti* cells**
991 *Chlamydomonas* cells were sediment on Poly-D-Lysine coated-12mm coverslips
992 (Menzel Glaser) for 30min prior to 7min fixation in -20°C methanol. Cells were washed
993 in PBS then incubated in 1% bovine serum albumin (BSA) in PBS-T with primary

994 antibodies against POC16 (1:500), Bld12 (1:100) and Tubulin DM1α (1:500) for 1h at
995 room temperature. Coverslips were washed in PBS for 30min prior to incubation with
996 secondary antibodies for 1 hour at room temperature, washed again for 30min in PBS
997 and mounted in DAPCO mounting medium containing DAPI (Abcam). Only isolated
998 cells were analyzed, the rest of the cells, which were grouped in palmeloids were not
999 analyzed.
1000 Imaging was performed on a Zeiss LSM700 confocal microscope with a PlanApo 63x
1001 oil immersion objective (NA 1.4) and optical sections were acquired every 0.33 nm,
1002 then projected together using ImageJ.
1003
1004 **Electron microscopy on *Chlamydomonas reinhardtii***
1005 For sample preparation, cells were pelleted for 5min at 500g, fixed in 2.5%
1006 glutaraldehyde/TAP 1X for 1h at RT and washed 3x in TAP 1X. Fixed cells were
1007 further treated with 2% osmium tetraoxyde in buffer and immersed in a solution of
1008 uranyl acetate 0.25% over night (Tandler reference) to enhance contrast of membranes.
1009 The pellets were deshydrated in increasing concentrations of ethanol followed by pure
1010 propylene oxide and embedded in Epon resin. Thin sections for electron microscopy
1011 were stained with uranyl acetate and lead citrate, and observed in a Technai 20 electron
1012 microscope (FEI Company).
1013 Micrographs analyses were performed on ImageJ and GraphPadPrism7.
1014 Symmetrization on top views was performed using CentrioleJ pluggin (https://gonczy-
1015 lab.epfl.ch/resources/ressources-centriolej/). The UnwarpJ plugin was required to
1016 perform image circularization using the center of the nine A-microtubules as landmark
1017 points. A 9-fold symmetrization was then applied to the circularized image. The
1018 deformation parameters were adjusted depending on the quality of the original image.

1019 For WT: initial deformation → fine, final deformation → fine. For m504: initial
1020 deformation→ fine, final deformation→ very fine.
1021
1022 **Image analysis**
1023 For centrioles counting, immunofluorescences were analyzed on a Leica
1024 epifluorescence microcoscope.
1025 For fluorescence intensity, maximal projections were used.
1026
1027 Confocal centrosomal intensities were assessed using an area of 20 pixels on Fiji. For
1028 each experiment, control values were averaged and all individual measures for control
1029 and treated conditions were normalized accordingly to obtain the relative intensity
1030 (A.U.). Normalized individual values were plotted on GraphPadPrism7.
1031
1032 Confocal centriolar intensities were assessed by individual plot profil (25 points) on
1033 each pair of mature centrioles. For each experiment, the average (Av) of control values
1034 was calculated and all individual measures for control and treated conditions were
1035 normalized on Av to obtain the relative intensity (A.U.). An average of all normalized
1036 measures was generated and plotted in GraphPadPrism7.
1037
1038 For U-ExM data, length coverage quantification was performed as previously published
1039 in (Le Guennec et al., 2020).
1040 For top views, a measurement from the exterior to the interior of the centriole was
1041 performed on each microtubule triplet displaying a resolved signal for both tubulin and
1042 the core protein. For each tubulin measurement, the position (x-value) of the maximal
1043 fluorescence intensity of the core protein was aligned individually to the position of the

1044 respective tubulin maximal intensity. All individual values of distance were plotted and
1045 analyzed in GraphPadPrism7.
1046 Measurements of diameter in siControl and siWDR90 conditions were performed on
1047 S-phase mature centrioles imaged in lateral view. Briefly, lines of 50 pixels thickness
1048 were drawn within the proximal, central and distal regions defined in respect with the
1049 position of inner core proteins POC5 and FAM161A. Proximal region was then defined
1050 as the portion of the centriole below staining of POC5 or FAM161A and the distal
1051 region as above. In the siWDR90 condition, proximal region was defined as below the
1052 remaining belt of POC5 of FAM161A, the core region was measured just above the
1053 remaining belt and the distal region as the last 100 nm of the centriole. The Fiji plot
1054 profile tool was used to obtain the fluorescence intensity profile from proximal to distal
1055 for tubulin and the core protein from the same line scan.
1056 Roundness was calculated on perfectly imaged top views of centrioles by connecting
1057 tubulin peaks on ImageJ.
1058
1059 **Statistical analysis**
1060
1061 The comparison of two groups was performed using a two-sided Student's t-test or its
1062 non parametric correspondent, the Mann-Whitney test, if normality was not granted
1063 either because not checked ($n < 10$) or because rejected (D'Agostino and Pearson test).
1064 The comparisons of more than two groups were made using one or two ways ANOVAs
1065 followed by post-hoc tests (Holm Sidak's or Sidak's) to identify all the significant
1066 group differences. N indicates independent biological replicates from distinct sample.
1067 Every experiment, except for resin electron microscopy, was performed at least 3 times
1068 independently. Data are all represented as scatter or aligned dot plot with centerline as

1069 mean, except for percentages quantifications, which are represented as histogram bars.
1070 The graphs with error bars indicate 1 SD (+/-) and the significance level is denoted as
1071 usual (*p<0.05, **p<0.01, ***p<0.001, ****p<0.0001). All the statistical analyses
1072 were performed using Excel or Prism7 (Graphpad version 7.0a, April 2, 2016).
1073

1074 **Supplemental methods**

1075 **Protein alignment**

1076 The protein sequences were aligned using Clustal Omega and the secondary structure
1077 elements were predicted using Phyre 2, PONDR and XtalPred-RF.
1078

1079 **3D model**

1080 The *Chlamydomonas* POC16 model was prepared using *Phyre2* (Kelley 2015 Nature
1081 Protocols) and refined against the FAP20 cryo-EM map EMD_20858 using
1082 *phenix.real_space_refine* (Afonine 2018 ActaD). Superposition of the POC16 model
1083 excluding flexible loops against FAP20 was done using *COOT* (Emsley 2010 ActaD)
1084 and yielded a Root Mean Square Deviation (RMSD) value of 1.6 Angs. The figures
1085 were prepared using *ChimeraX* (Goddard 2018 Protein Science).
1086

1087 **PtPOC16 antibody purification**

1088 To generate anti-PtPOC16 antibody, a fragment encoding amino acids 2-210 was used
1089 for rabbit immunization (Eurogentec). Antibodies were subsequently affinity-purified
1090 over a column of PtPOC16(2-210) immobilized on Affi-Gel 10 (Bio-Rad Laboratories)
1091 and dialyzed against PBS/5% glycerol.
1092

1093 **Immunofluorescence in *Paramecium tetraurelia***

1094 Immunofluorescence was performed according to (Beisson et al., 2010). Briefly,
1095 Paramecia were permeabilized for 5min in 0.5% saponin in PHEM Buffer (PIPES
1096 60mM, HEPES 25mM, EGTA 10mM, 2mM MgCl2 pH 6.9) and fixed in 2%
1097 paraformaldehyde (PFA) for 10 min. Cells were washed 3x10min in PHEM-saponin
1098 buffer and stained with primary antibodies against POC16 (1:50) and tubulin 1D5
1099 (1:10) for 30min at room temperature. Cells were incubated with secondary antibodies
1100 for 20min, washed twice in PHEM-saponin prior to a last wash in TBST-BSA
1101 supplemented with Hoechst 2mg/mL.
1102 Imaging was performed on a Zeiss LSM700 confocal microscope with a PlanApo 40x
1103 oil immersion objective (NA 1.4) and optical sections were acquired every 0.33 m,
1104 then projected together using ImageJ.
1105
1106 **Human cells cold shock treatment**
1107 U2OS cells grown on 15mm coverslips and transiently overexpressing mCherry-
1108 WDR90-N(1-225)RR for 24hrs were placed in 4°C PBS for an hour on ice and fixed in
1109 -20°C methanol. Coverslips were processed for immunofluorescence using primary
1110 antibodies against mCherry (1:500) and anti-tubulin DM1α (1:1000).
1111
1112 ***In vitro* crPOC16 microtubule decoration**
1113 *In vitro* stabilized Taxol-microtubules were prepared in MES-BRB80 derived buffer in
1114 contrast to K-PIPES-BRB80 to allow crPOC16(1-295) protein solubility. Samples were
1115 then processed similarly to WDR90-N(1-225).
1116
1117
1118

1119 **FACS analysis**

1120 Cells were processed similarly to Macheret et al 2018. Post-mitotic cells were washed
1121 2x with PBS then permeabilized and treated with Click-EdU-Alexa 647 (Carl Roth EdU
1122 Click FC-647, ref 7783.1) according to manufacturer's instruction. Genomic DNA was
1123 stained with propidium iodide (Sigma, Cat. No. 81845) in combination with RNase
1124 (Roche, Cat. No. 11119915001). EdU-DNA content profiles were acquired by flow
1125 cytometry (Gallios, Beckman Coulter) to assess the percentage of cells that entered S
1126 phase in each condition at each time point.

1127

1128 **PCM1 depletion using siRNA**

1129 Stable inducible GFP-WDR90 U2OS cells were plated in doxycycline containing–
1130 medium onto 15mm coverslips in a 6 well plate and 20nM silencer select pre-designed
1131 siRNA ADCSU9L was transfected using Lipofectamine RNAimax (Thermo Fischer
1132 Scientific). Medium was changed 4hrs post-transfection and cells were analyzed 48
1133 hours post-transfection.

1134

1135

1136 **Contact for reagent and resource sharing**

1137 Further information and requests for resources and reagents should be directed to and
1138 will be fulfilled by the Lead Contact, Virginie Hamel (virginie.hamel@unige.ch).

1139

1140

1141 **References**

1142 Azimzadeh J, Hergert P, Delouvée A, Euteneuer U, Formstecher E, Khodjakov A,
1143 Bornens M. 2009. hPOC5 is a centrin-binding protein required for assembly of
1144 full-length centrioles. *J Cell Biol* **185**:101–114. doi:10.1083/jcb.200808082

1145 Beisson J, Bétermier M, Bré MH, Cohen J, Duharcourt S, Duret L, Kung C, Malinsky
1146 S, Meyer E, Preer JR, Sperling L. 2010. Immunohistochemistry of paramecium
1147 cytoskeletal structures. *Cold Spring Harb Protoc* **5**:pdb.prot5365-pdb.prot5365.
1148 doi:10.1101/pdb.prot5365

1149 Bornens M. 2012. The centrosome in cells and organisms. *Science* **335**:422–6.
1150 doi:10.1126/science.1209037

1151 Breslow DK, Holland AJ. 2019. Mechanism and Regulation of Centriole and Cilium
1152 Biogenesis. *Annu Rev Biochem* **88**:691–724. doi:10.1146/annurev-biochem-
1153 013118-111153

1154 Conduit PT, Wainman A, Raff JW. 2015. Centrosome function and assembly in
1155 animal cells. *Nat Rev Mol Cell Biol* **16**:611–624. doi:10.1038/nrm4062

1156 Drew K, Lee C, Huizar RL, Tu F, Borgeson B, McWhite CD, Ma Y, Wallingford JB,
1157 Marcotte EM. 2017. Integration of over 9,000 mass spectrometry experiments
1158 builds a global map of human protein complexes. *Mol Syst Biol* **13**:932.
1159 doi:10.15252/msb.20167490

1160 Dymek EE, Lin J, Fu G, Porter ME, Nicastro D, Smith EF. 2019. PACRG and FAP20
1161 form the inner junction of axonemal doublet microtubules and regulate ciliary
1162 motility. *Mol Biol Cell* **30**:1805–1816. doi:10.1091/mbc.e19-01-0063

1163 Gambarotto D, Zwettler FU, Guennec M Le, Schmidt-cernohorska M, Fortun D,
1164 Borgers S, Heine J, Schloetel J, Reuss M, Unser M, Boyden ES, Sauer M, Hamel

1165 V, Guichard P. 2019. Imaging cellular ultrastructures using expansion
1166 microscopy (U-ExM). *Nat Methods* **16**. doi:10.1038/s41592-018-0238-1
1167 Geimer S, Melkonian M. 2004. The ultrastructure of the Chlamydomonas reinhardtii
1168 basal apparatus: identification of an early marker of radial asymmetry inherent in
1169 the basal body. *J Cell Sci* **117**:2663–74. doi:10.1242/jcs.01120
1170 Gibson DG, Young L, Chuang R-Y, Venter JC, Hutchison CA, Smith HO. 2009.
1171 Enzymatic assembly of DNA molecules up to several hundred kilobases. *Nat*
1172 *Methods* **6**:343–345. doi:10.1038/nmeth.1318
1173 Gönczy P. 2015. Centrosomes and cancer: revisiting a long-standing relationship. *Nat*
1174 *Rev Cancer* **15**:639–52. doi:10.1038/nrc3995
1175 Hamel V, Steib E, Hamelin R, Armand F, Borgers S, Flückiger I, Busso C, Olieric N,
1176 Sorzano COS, Steinmetz MO, Guichard P, Gönczy P. 2017. Identification of
1177 Chlamydomonas Central Core Centriolar Proteins Reveals a Role for Human
1178 WDR90 in Ciliogenesis. *Curr Biol* **27**:2486-2498.e6.
1179 doi:10.1016/j.cub.2017.07.011
1180 Ishikawa H, Marshall WF. 2011. Ciliogenesis: Building the cell's antenna. *Nat Rev*
1181 *Mol Cell Biol* **12**:222–234. doi:10.1038/nrm3085
1182 Khalifa A, Ichikawa M, Dai D, Kubo S, Black C, Peri K, McAlear TS, Veyron S,
1183 Yang SK, Vargas J, Bechstedt S, Trempe J-F, Bui KH. 2019. The inner junction
1184 complex of the cilia is an interaction hub that involves tubulin post-translational
1185 modifications. *bioRxiv* 774695. doi:10.1101/774695
1186 Khalifa AAZ, Ichikawa M, Dai D, Kubo S, Black CS, Peri K, McAlear TS, Veyron S,
1187 Yang SK, Vargas J, Bechstedt S, Trempe JF, Bui KH. 2020. The inner junction
1188 complex of the cilia is an interaction hub that involves tubulin post-translational
1189 modifications. *Elife* **9**:1–25. doi:10.7554/eLife.52760

1190 Klena N, Gambarotto D, Le Guennec M, Borgers S, Guichard P, Hamel V. 2018.
1191 Isolation and Fluorescence Imaging for Single-particle Reconstruction of
1192 Chlamydomonas Centrioles. *JoVE* e58109. doi:doi:10.3791/58109
1193 Le Guennec M, Klena N, Gambarotto D, Laporte MH, Tassin A, van den Hoek H,
1194 Erdmann PS, Schaffer M, Kovacik L, Borgers S, Goldie KN, Stahlberg H,
1195 Bornens M, Azimzadeh J, Engel BD, Hamel V, Guichard P. 2020. A helical
1196 inner scaffold provides a structural basis for centriole cohesion. *Sci Adv*
1197 **6**:eaaz4137. doi:10.1126/sciadv.aaz4137
1198 Li X, Zhang R, Patena W, Gang SS, Blum SR, Ivanova N, Yue R, Robertson JM,
1199 Lefebvre PA, Fitz-Gibbon ST, Grossman AR, Jonikas MC. 2016. An Indexed,
1200 Mapped Mutant Library Enables Reverse Genetics Studies of Biological
1201 Processes in *Chlamydomonas reinhardtii*. *Plant Cell* **28**:367–387.
1202 doi:10.1105/tpc.15.00465
1203 Ma M, Stoyanova M, Rademacher G, Dutcher SK, Brown A, Zhang R. 2019.
1204 Structure of the Decorated Ciliary Doublet Microtubule. *Cell* **179**:909-922.e12.
1205 doi:10.1016/j.cell.2019.09.030
1206 Marteil G, Guerrero A, Vieira AF, De Almeida BP, Machado P, Mendonça S,
1207 Mesquita M, Villarreal B, Fonseca I, Francia ME, Dores K, Martins NP, Jana
1208 SC, Tranfield EM, Barbosa-Morais NL, Paredes J, Pellman D, Godinho SA,
1209 Bettencourt-Dias M. 2018. Over-elongation of centrioles in cancer promotes
1210 centriole amplification and chromosome missegregation. *Nat Commun* **9**.
1211 doi:10.1038/s41467-018-03641-x
1212 Nakazawa Y, Hiraki M, Kamiya R, Hirono M. 2007. SAS-6 is a cartwheel protein
1213 that establishes the 9-fold symmetry of the centriole. *Curr Biol* **17**:2169–2174.
1214 Nigg EA, Holland AJ. 2018. Once and only once: Mechanisms of centriole

duplication and their deregulation in diseases. *Nat Rev Mol Cell Biol* **19**:297–312. doi:10.1038/nrm.2017.127

Nigg EA, Raff JW. 2009. Centrioles, centrosomes, and cilia in health and disease. *Cell* **139**:663–678.

Nizak C, Martin-Lluesma S, Moutel S, Roux A, Kreis TE, Goud B, Perez F. 2003. Recombinant antibodies against subcellular fractions used to track endogenous Golgi protein dynamics in vivo. *Traffic* **4**:739–53. doi:10.1107/S0907444912048664

O'Toole ET, Giddings TH, McIntosh JR, Dutcher SK. 2003. Three-dimensional Organization of Basal Bodies from Wild-Type and δ-Tubulin Deletion Strains of Chlamydomonas reinhardtii. *Mol Biol Cell* **14**:2999–3012. doi:10.1091/mbc.e02-11-0755

Owa M, Uchihashi T, Yanagisawa H aki, Yamano T, Iguchi H, Fukuzawa H, Wakabayashi K ichi, Ando T, Kikkawa M. 2019. Inner lumen proteins stabilize doublet microtubules in cilia and flagella. *Nat Commun* **10**:1–10. doi:10.1038/s41467-019-09051-x

Pearson CG, Osborn DPS, Giddings TH, Beales PL, Winey M. 2009. Basal body stability and ciliogenesis requires the conserved component Poc1. *J Cell Biol* **187**:905–920. doi:10.1083/jcb.200908019

Schmidt-Cernohorska M, Zhernov I, Steib E, Le Guennec M, Achek R, Borgers S, Demurtas D, Mouawad L, Lansky Z, Hamel V, Guichard P. 2019. Flagellar microtubule doublet assembly in vitro reveals a regulatory role of tubulin C-terminal tails. *Science*.

Strnad P, Leidel S, Vinogradova T, Euteneuer U, Khodjakov A, Gönczy P. 2007. Regulated HsSAS-6 levels ensure formation of a single procentriole per centriole

1240 during the centrosome duplication cycle. *Dev Cell* **13**:203–13.
1241 doi:10.1016/j.devcel.2007.07.004
1242 Tanos BE, Yang H-J, Soni R, Wang W-J, Macaluso FP, Asara JM, Tsou M-FB. 2013.
1243 Centriole distal appendages promote membrane docking, leading to cilia
1244 initiation. *Genes Dev* **27**:163–8. doi:10.1101/gad.207043.112
1245 Venoux M, Tait X, Hames RS, Straatman KR, Woodland HR, Fry AM. 2013. Poc1A
1246 and Poc1B act together in human cells to ensure centriole integrity. *J Cell Sci*
1247 **126**:163–175. doi:10.1242/jcs.111203
1248 Wang JT, Kong D, Hoerner CR, Loncarek J, Stearns T. 2017. Centriole triplet
1249 microtubules are required for stable centriole formation and inheritance in
1250 human cells. *Elife* **6**:1–17. doi:10.7554/eLife.29061
1251 Xu C, Min J. 2011. Structure and function of WD40 domain proteins. *Protein {&}*
1252 *cell* **2**:202–214. doi:10.1007/s13238-011-1018-1
1253 Yanagisawa H, Mathis G, Oda T, Hirono M, Richey EA, Ishikawa H, Marshall WF,
1254 Kikkawa M, Qin H. 2014. FAP20 is an inner junction protein of doublet
1255 microtubules essential for both the planar asymmetrical waveform and stability
1256 of flagella in Chlamydomonas. *Mol Biol Cell* **25**:1472–83.
1257 doi:10.1091/mbc.E13-08-0464
1258 Yanagisawa HA, Mathis G, Oda T, Hirono M, Richey EA, Ishikawa H, Marshall WF,
1259 Kikkawa M, Qin H. 2014. FAP20 is an inner junction protein of doublet
1260 microtubules essential for both the planar asymmetrical waveform and stability
1261 of flagella in Chlamydomonas. *Mol Biol Cell* **25**:1472–1483.
1262 doi:10.1091/mbc.E13-08-0464
1263 Zach F, Grassmann F, Langmann T, Sorusch N, Wolfrum U, Stöhr H. 2012. The
1264 retinitis pigmentosa 28 protein FAM161A is a novel ciliary protein involved in

1265 intermolecular protein interaction and microtubule association. *Hum Mol Genet*
1266 **21**:4573–4586. doi:10.1093/hmg/dds268
1267
1268